C.P. No. 1315

C.P. No. 1315

PROCUREMENT EXECUTIVE, MINISTRY OF DEFENCE

AERONAUTICAL RESEARCH COUNCIL

CURRENT PAPERS

Free-Flight Model Dynamic Stability Measurements on a 'Not-so Slender' Wing/Fin combination at Zero and Small Lift, M= 0.8 to 2.0

by

G. H. Greenwood and Geraldine F. Edwards

Aerodynamics Dept., R.A.E., Farnborough

LONDON: HER MAJESTY'S STATIONERY OFFICE

1975

PRICE £1-40 NET

UDC 533.695.14 : 533.6.013.412 : 533.6.013.413 : 533.6.055

*CP No.1315
April 1974

FREE-FLIGHT MODEL DYNAMIC STABILITY MEASUREMENTS ON A 'NOT-SO-SLENDER' WING/FIN COMBINATION AT ZERO AND SMALL LIFT, M = 0.8 TO 2.0

by

G. H. Greenwood
Geraldine F. Edwards

SUMMARY

Dynamic longitudinal and lateral stability measurements for a 'not-so-slender' wing plus fin have been made in free flight at zero and small lift. Agreement between experiment and theory is generally good but exceptions were found in the magnitude and variation of the pitching moment derivative m_w and the pitch-damping derivative $m_{\dot{\theta}}$. The effect of adding a small fairing in simulation of the support-sting shroud on complementary wind-tunnel models appears to be confined to m_w, n_v and y_v .

---

* Replaces RAE Technical Report 74054 - ARC 35501

CONTENTS

		Page
1	INTRODUCTION	3
2	EXPERIMENTAL METHOD	4
3	DESCRIPTION OF THE MODELS	5
4	THEORETICAL ESTIMATES OF STABILITY DERIVATIVES	7
	4.1 Basic configuration	7
	4.2 Modified configuration	7
5	RESULTS	8
	5.1 Basic model at zero lift (models 1 and 5)	8
	5.1.1 z_w	8
	5.1.2 m_w	8
	5.1.3 $m_{\dot{\theta}}$	9
	5.1.4 y_v	9
	5.1.5 n_v	10
	5.1.6 ℓ_v	10
	5.1.7 ℓ_p	10
	5.1.8 $(n_r - n_{\dot{v}})$	10
	5.1.9 Manoeuvre margin	11
	5.2 Basic model at lift (model 3)	11
	5.3 Modified model at zero lift (models 4 and 6)	12
6	CONCLUSIONS	14
Appendix A	Equations of motion used in digital analysis	17
Appendix B	Estimation methods	18
Tables 1 and 2		25
Symbols		27
References		30
Illustrations		Figures 1-26

1 INTRODUCTION

In recent years there has been a great deal of research on the aerodynamics of slender wings, mainly directed toward the design of supersonic transport aircraft. As part of the research into the dynamic stability of slender wings, free-flight model tests were made at RAE on a wing/fin configuration code-named Orion which was later adopted as the AGARD 'G' standard research model. These tests, at zero lift, are reported in Ref.1 and further tests on this configuration at zero and moderate lift are reported in Ref.2. The planform of Orion was chosen as being typical of a range of configurations being studied in the context of supersonic transport, but at the same time it was simple enough to be amenable to theoretical treatment.

To further our knowledge of such wing shapes it was decided to extend the Orion tests to include a 'not-so-slender' wing having possible application to transport and fighter aircraft. This model, named Viking, has the same leading-edge specification, *viz.* straight to 2/3 chord and parabolic thereafter to streamwise tips, and the same normal leading-edge angle, but its aspect ratio is 1.385 compared with 0.865 for Orion.

The Viking configuration was agreed jointly by RAE and FFA* Sweden and the proposed test programme, to provide static and dynamic aerodynamic derivatives at subsonic through to supersonic speeds, included free-flight model and wind-tunnel tests at RAE and wind-tunnel tests at FFA.

Although covering a wide Mach number range (0.8 to 2.0), the emphasis of the free-flight model tests was on providing data for assessing the reliability of wind-tunnel results in the transonic speed range.

Because of the need for directional stability the free-flight models were fin stabilised and the resulting wing/fin combination was adopted as the common shape for all the associated wind-tunnel tests. Conversely, the need for model support stings in the wind-tunnel tests led to the fitting of simulated support fairings on two of the free-flight models to assess the effect of these on the dynamic data.

The present report contains the stability derivatives** from the free-flight model tests and comparison is made with theoretical estimates.

---

* Flygtekniska Föröksanstalten - the Aeronautical Research Institute of Sweden.

** Because the present tests are an extension of the Orion tests it was considered logical to use the same notation for the stability derivatives as used in Refs.1 and 2; the relation to the new notation of Ref.32 is given in Table 2.

Measurements are presented of z_w, m_w, $m_{\dot{\theta}}$, n_v, y_v, ℓ_v, ℓ_p, $(n_r - n_{\dot{v}})$ and manoeuvre margin; values of ℓ_{vw} are not presented because of large scatter in the measurements of this derivative.

A more comprehensive report will be issued later containing comparisons between free-flight and RAE and FFA[33] wind-tunnel test results.

2 EXPERIMENTAL METHOD

The various applications of the RAE free-flight rocket-propelled model technique have been described fully elsewhere; Ref.3 perhaps gives the best overall picture of the method. However, for completeness, a brief description of the technique as applied in the specific field of stability measurements is given here.

For such measurements the model was mounted on a solid-fuel rocket motor (see Fig.4) and accelerated to the desired maximum test speed over a test range (Aberporth, in the present instance) and then, when the thrusting phase was over, the model was allowed to separate from the inert motor and coast in free flight. During this coasting phase non-lifting models provided with adequate directional stability will follow a ballistic trajectory.

When measurements were required at non-zero angles-of-attack, i.e. under lifting conditions (as for model 3 in the present tests), a potential range hazard was avoided by inducing the model to roll; this combination of lift and roll resulted in a large-radius barrel roll motion which remained centred on an acceptable trajectory within the range safety limits.

The basis of the stability measurement was the analysis of several oscillations which were induced by igniting short-duration (0.07 second) pulse rockets at predetermined intervals during the post-separation coasting phase. These pulse rockets, ignited by an internal electro-mechanical switch, thrust approximately at right-angles to the model longitudinal axis and could be operated to give either predominately longitudinal or lateral oscillatory modes. In the present tests six oscillations were induced in each test flight but it was also possible to analyse the oscillation resulting from the separation of the model from its rocket motor.

The oscillatory responses resulting from the in-flight disturbances were sensed by internal accelerometers. These measurements were radio-telemetered to a range station and recorded on magnetic tape. This record was subsequently analysed by a digital technique developed by Waterfall[4]. This is essentially a least-squares curve-fitting procedure in which estimated initial values of the

aerodynamic derivatives are improved iteratively by a computer program to values giving a best fit to the measured response data. The equations of motion constituting the basic mathematical model assumed for the responses are given in Appendix A and the estimated values of n_p and ℓ_r used in the analysis are given in Fig.8. This method takes due account of non-linear coupling effects between the longitudinal and lateral motions, which distinguishes it from the older graphical time-vector technique used in Ref.1 for the early free-flight Orion models.

In the present free-flight model tests the emphasis was on measurements in the transonic speed range, this being perhaps the most difficult regime for the wind-tunnel meauurements. At these speeds the stability derivatives may be expected to change rapidly with Mach number, and since the free-flight measurements are based on the analysis of several cycles of each induced oscillation it follows that if the Mach number interval over this analysis period can be reduced, a greater accuracy in the derivative/Mach number relationship will result. On the more recent Orion tests of Ref.2 this problem was tackled by selecting flight trajectories in which the model drag and gravity forces were in near balance at transonic speeds, so that Mach number changed only slowly near $M = 1.0$. This particular technique is described fully in Ref.5 and was adopted for the present tests.

The space coordinates and the velocity of the coasting models were obtained by the usual weapons-range techniques, e.g. kinetheodolite, radar and radio-Doppler trackings. The wind speed and direction, atmospheric pressure and temperature at the flight altitudes were obtained by radiosonde measurements.

All these range measurements were combined in a computer program[4] with the output from the model-borne instrumentation to give in-flight angles-of-attack, drag and lift coefficients together with Mach number and dynamic pressure.

3 DESCRIPTION OF THE MODELS

Fig.1 and Table 1 give details of the basic configuration of the Viking free-flight models and Fig.2 shows the configuration modified by the addition of a fairing simulating the shroud over the support sting of the complementary wind-tunnel models. Photographs of a basic and a modified model are presented in Fig.3 and a photograph of a model mounted on its rocket-motor in its launching condition (see section 2) is presented in Fig.4.

Each model was constructed using a stiff light-alloy centre-plate which conformed to the wing planform and which was chamfered to give sharp leading and trailing edges. Glass-fibre reinforced mouldings were bonded to the top and

bottom of the plate to give the wing the required external profile, leaving sufficient cut-outs in the plate and mouldings to house the telemetry equipment, instrumentation and disturbance rockets. These cut-outs were finally covered by removable hatches profiled to the local external shape. The light-alloy stabilising fin was rigidly secured to the centre plate and the radio-telemetry transmission aerial[6] was attached to the trailing edge.

Each model was instrumented to measure the following quantities:

(1) Normal and lateral accelerations at the centre-of-gravity

(2) Normal and lateral accelerations at a station aft of the centre-of-gravity

(3) Angular acceleration in roll

(4) Angle of bank (by magnetometer)

(5) Longitudinal acceleration

(6) Pitot pressure (to provide an additional check on the range measurements of velocity and altitude)

In addition to the above, the lifting model (3) was fitted with a differential-pressure nose probe to measure angle of attack in pitch and yaw.

Care was taken to ensure that each model was ballasted to give a launching mass consistent with the trajectory requirement for sustained transonic flight described in Ref.5 (see section 2) and each model was balanced to give a centre-of-gravity position at 0.5 centre-line chord. Pre-flight measurements[7] were also made of the moments of inertia of each model in pitch, roll and yaw and of the product of inertia (Ixz). Values of model mass and inertia are included in Table 1.

A total of six Viking free-flight models were tested, but one broke up at separation from its rocket motor giving no results. The remaining five consisted of two models of the basic configuration of Fig.1 (models 1 and 5) and two of the modified configuration of Fig.2 (models 4 and 6), all tested at nominally zero lift; the remaining model was the basic configuration tested at moderate lift (model 3). This latter model had elevators (Fig.1 and Table 1) set at 5.5 degrees on the port side and 4.5 degrees in the same direction on the starboard side to give the model a nose-up trim. The differential setting of one degree between port and starboard elevators was to induce the lifting model 3 to perform a large-radius barrel roll about its mean flight trajectory to confine it within the safety limits of the firing range (see section 2).

4 THEORETICAL ESTIMATES OF STABILITY DERIVATIVES

4.1 Basic configuration (Fig.1)

For the most part the same methods as those described in Ref.1 have been used for the theoretical estimates. In order to make use of existing theoretical and experimental data compiled for wings with straight leading edges and streamwise tips an 'equivalent' cropped delta planform was substituted when necessary for the real wing; the slenderness ratio $s/c_0 = 0.4$ and $A \tan \Lambda_0 = 2.891$ being kept the same for the real and 'equivalent' wings. This gave an 'equivalent' wing only slightly different from the real wing *viz.* $\Lambda_0 = 64.5$ degrees (64.4 real wing), $A = 1.379$ (1.385) and $S = 0.959 m^2$ ($0.955\ m^2$) . In the estimates of the lateral derivatives a similar simplification of the fin planform was also made when necessary.

For the tests at nominally zero lift, fully attached flow at the leading edges may be assumed, and non-linear components of the derivatives ignored. In the application of linearised theories the wing and fin were first considered separately and then corrections for mutual interference effects were applied to the results.

A detailed description of the theoretical methods used to obtain the individual derivatives is given in Appendix B.

4.2 Modified configuration (Fig.2)

The difference between the basic and modified shape is confined to a relatively small portion of the models, as seen in Figs.2 and 3.

The effect of this small modification on the various derivatives has been calculated by slender body theory[8] and is summarised below as a percentage of the derivative appropriate to the unmodified shape estimated by the same theory.

$\underline{z_w}$ - modification gives a decrease of 1.4%

$\underline{m_w}$ - an increase of 5%

$\underline{m_{\dot{\theta}}}$ - a decrease of 1.4%

$\underline{y_v}$ - an increase of 5%

$\underline{n_v}$ - an increase of 2%

$\underline{\ell_v}$ - an increase of 56%*

---

* Because of the small absolute value of ℓ_v , this increase is in fact comparable in magnitude to the experimental scatter in the measurements (see Fig.24).

$\frac{(n_r - n_v)}{\ell_p}$ - an increase of 12%

- an increase of 2%

5 RESULTS

The variation of free-stream Reynolds number with Mach number for all the models is given in Fig.5. Measurements of the stability derivatives and the corresponding estimated values are shown in Figs.9 to 26.

Some of the derivatives are plotted with a vertical line indicating the magnitude of the likely error in computing[4] the derivative. This is effectively a measure of the range of values of the derivative which gives the same accuracy in fitting the computed responses to the measured responses. It does not necessarily indicate the total probable error in the derivative since this also depends upon other factors such as instrument errors, uncertainties in the meteorological measurements, model speed and tracking errors etc. The vertical limits in the plotted data do, however, give a guide to the relative accuracies of the computed derivatives; absence of limits implies that the likely error is within the height of the plotting symbol.

5.1 Basic model at zero lift (models 1 and 5)

Although models 1 and 5 were intended to fly at zero lift they in fact trimmed at a small angle of attack and small C_L, as seen in Fig.6; the maximum angle of attack was about 1 degree at subsonic speeds and generally less than $\frac{1}{4}$ degree at supersonic speeds.

5.1.1 z_w (Fig.9)

At $M \leqslant 1.01$ the trimmed angle of attack for all the models was larger than at supersonic speeds (Fig.6) and to allow for possible lifting effects in z_w the measured values at $M \leqslant 1.01$ have been corrected in Fig.9 to values appropriate to zero-lift conditions using equation (B-2). This has done little, however, to remove the large scatter in this speed range, and so it is difficult to judge the efficacy of the theoretical methods.

At transonic and supersonic speeds the estimates from Refs.9 and 10 are greater than the mean experimental level by between about 5 to 15 per cent.

5.1.2 m_w (Fig.9)

At $M \leqslant 1.012$ the measured values of m_w have been corrected to values appropriate to a zero trim angle of attack using equation (B-5) and the measured α_T from Fig.6 (models 1 and 5). Fig.9 shows that at $M = 0.9$ these corrected

values of m_w give reasonable agreement with the estimates from Ref.11 with added thickness effects (equation (B-3)) but near $M = 1.0$, theory[8,10] has underestimated the experimental levels by about 40 per cent.

At $M = 1.12$ and 1.23 there is good agreement with the theory of Ref.9 with added thickness effects, but there is an increasing discrepancy with Mach number, and at $M = 1.9$ the theoretical estimate is 30 per cent more than the experimental values. Closer agreement between experiment and theory at speeds above $M = 1.3$ is in fact achieved when thickness effects are ignored, as is shown by the thin wing estimates[9] in Fig.9; there still remains, however, a large disparity between experiment and theory in the general trend of Mach number dependency of m_w.

In the transonic region $(1.0 < M < 1.3)$ the theory of Ref.10 has failed to predict the measured values of m_w both in magnitude and in the variation with Mach number.

5.1.3 $m_{\dot{\theta}}$ (Fig.10)

At subsonic speeds the experimental values of pitch damping are about 30 per cent below the theoretical estimates based on Refs.12 and 13 and at $M = 1$ the experimental point is about 50 per cent of the slender body value[8].

At supersonic speeds the mean experimental level is between 30 to 35 per cent below the supersonic linearised theory of Refs.14 and 15. Thickness effects may well account for part of these experimental/theoretical differences.

The general trend of the experimental results would seem to disprove the theoretical prediction of peak damping at or near sonic speeds; it will be seen later that this trend persists also for the lifting and the modified models of the present tests (Figs.16 and 22).

5.1.4 y_v (Fig.11)

At subsonic speeds there is fair agreement between experimental y_v and theory based on the lift curve slope of the equivalent cropped delta planform of the reflected fin as estimated from Ref.11.

At low supersonic speeds the 'not-so-slender' theory of Ref.10, using the 'modified gothic' planform of the reflected fin, has over-estimated y_v by about 20 to 25 per cent between $M = 1.1$ and 1.2.

For supersonic speeds $(M > 1.2)$ the mean experimental level is between 10 and 15 per cent below the estimates based on the lift-curve slope of the cropped delta planform of the reflected fin from Ref.9.

5.1.5 n_v (Fig.11)

At subsonic speeds the theoretical[11] estimate of n_v is within the general scatter of the experimental values.

At supersonic speeds theory based on Ref.9 has over-estimated the measured values by between 10 and 15 per cent, a similar discrepancy to the values for y_v.

5.1.6 ℓ_v (Fig.12)

At $M > 1.2$ the experimental values of ℓ_v are reasonably consistent with the combined theory of Refs.9 and 16, the former representing the direct fin effect and the latter the fin/wing interference effect on ℓ_v.

At $M < 1.2$ the experimental data have been corrected to values appropriate to zero trim angle of attack using the expression for lifting effects $\Delta\ell_v = \ell_{vw}\alpha_T$ given in section B.6, where ℓ_{vw} is the estimated value from Ref.17 and α_T is the measured trim angle of attack from Fig.6. These corrected values of ℓ_v are seen in Fig.12 to be generally in fair agreement with the theoretical trend indicated by the above supersonic theories[9,16] and the slender body values at $M = 1$ from Refs.8 and 18.

5.1.7 ℓ_p (Fig.12)

The damping derivatives are the most difficult to extract from the basic experimental data and inasmuch may contain greater uncertainties. If the amplitude of the induced lateral oscillation is small, then satisfactory reduction of ℓ_p is unlikely. For this reason, only two data points for model 1 and five for model 5 have been presented in Fig.12.

Owing to the uncertainty in reducing this derivative the experimental points for ℓ_p seen in Fig.12 show considerable scatter and the overall assessment of the data in Fig.12 must be that the results are all within about 25 per cent of the theoretical levels and that they tend to confirm the expected small variation in ℓ_p over the test speed range.

5.1.8 $(n_r - n_{\dot{v}})$ (Fig.13)

The large scatter at subsonic speeds in the experimental damping-in-yaw derivative precludes any useful comparison with theory. At supersonic speeds the scatter for the individual models is less, but there is a considerable difference in the measured damping between the nominally identical models 1 and

5 up to about $M = 1.4$. At about $M = 1.9$ agreement is good between models and would appear to be consistent with an extrapolation of the theoretical curves. In general, theory has overestimated the yaw damping at supersonic speeds.

5.1.9 Manoeuvre margin $(h - h_0/\bar{c})$ (Fig.14)

Theoretical and experimental values of the manoeuvre margin, $(h - h_0/\bar{c}) = m_w/z_w$, are shown in Fig.14; the theoretical estimates include thickness effects in m_w calculated from equation (B-3).

The differences between experiment and theory seen in Fig.14 reflect those for z_w and m_w seen in Fig.9.

The experimental aerodynamic centre is seen to be further aft than indicated by theory at $M < 1.2$ but the results in this speed range reflect the large uncertainties in the measured lift-curve slope in Fig.9. At higher speeds $(M > 1.2)$ the results are more reliable and indicate a forward movement of aerodynamic centre as Mach number increases, although this is not predicted by theory.

5.2 Basic model at lift (model 3)

The in-flight trimmed angle of attack for the lifting model (3) is given in Fig.7. This is seen as 3.5 degrees at $M = 0.8$, decreasing to 1 degree at $M = 1.0$, and it remains constant at this value for all supersonic speeds.

The only derivatives that may be expected to vary significantly with angle of attack are z_w, m_w, $m_{\dot{\theta}}$ and ℓ_v . The second-order derivatives used in calculating the increments due to angle of attack are given in the appropriate sections of Appendix B together with their derivations.

In Figs.15 to 20 the derivatives measured at zero lift (models 1 and 5) are compared directly with those measured on model 3 at lift.

The scatter in the measurements of z_w (Fig.15) at subsonic speeds is sufficient to mask any lifting effects if present. At supersonic speeds $(M > 1.2)$ the three experimental points for the lifting model 3 indicate an increase in z_w due to lift but the magnitude of this increase is obscured by the evident scatter in the lifting results.

A moderate increase in m_w at $M < 1.2$ (Fig.15) for the lifting model is largely accounted for by the estimated increment due to angle of attack $\Delta m_w = -1.58\alpha_T$ (equation (B-5)). At higher speeds the measured effect of angle

of attack on m_w is seen to be negligible, although the theory continues to predict the same moderate increase.

Fig.17 shows some increase in n_v and y_v due to angle of attack at transonic Mach numbers but above $M = 1.2$ the effect of angle of attack is negligible.

The comparisons for ℓ_v in Fig.18 also show an increase in this derivative at $M < 1.2$ for the lifting model. At higher speeds the general level of ℓ_v for the lifting model is again higher than that for the zero-lift models, but the magnitude of the increase is comparable with the scatter between individual models and must therefore be regarded as tentative.

Also shown in Fig.18 are the measured values of ℓ_v for the lifting model corrected to zero-lift conditions using the expression for the increment due to lift, $\Delta\ell_v = \ell_{vw}\alpha_T$, from section B.6. The failure of the correction to completely collapse the data from model 3 to the zero-lift data from models 1 and 5 may be due partly to the general technique uncertainties and partly to uncertainties in estimating[17] ℓ_{vw}. Nevertheless, the collapse is sufficiently good at transonic speeds to largely validate the estimation method of the increment due to lift, $\Delta\ell_v$, at these speeds.

The measured manoeuvre margin (Fig.20) shows no conclusive differences between the lifting and non-lifting models. There is, however, some indication that the mean experimental levels near $M = 1$ are consistent with a more rearward position of the aerodynamic centre for the lifting model which is in keeping with the increase in m_w seen in Fig.15.

The theoretical estimates[9,11] in Fig.20 include thickness effects (equation (B-3)) and lifting effects (equations (B-2), (B-5)) appropriate to α_T for the lifting model 3 (Fig.7).

For the remaining derivatives, $m_{\dot{\theta}}$ (Fig.16), ℓ_p (Fig.18) and $(n_r - n_{\dot{v}})$ (Fig.19) there are no conclusive differences due to angle of attack.

5.3 Modified model at zero lift (models 4 and 6)

Figs.21 to 26 show the results from the modified models (4 and 6) at zero lift compared with those from the basic models (1 and 5) at zero lift. Also shown are the estimated levels of the derivatives for the modified and basic shape at $M = 1$ calculated by slender body theory[8].

The comparisons of z_w in Fig.21 do not indicate any measurable differences in the derivative due to the modification. Those for m_w, corrected to values appropriate to $\alpha_T = 0$ (see section B.2), in Fig.21 do however show some increase between $M = 1.0$ and 1.2 for the modified model. In the absence of a measurable increase in z_w it is possible that this increase in m_w reflects a rearward movement in aerodynamic centre on the modified model in this speed range.

The yawing moment due to sideslip derivative, n_v (Fig.23), shows some increase for the modified model especially at supersonic speeds. Slender body theory predicts an increase of about 2 per cent due to the modification but the measured increase is generally greater at between 5 to 10 per cent for $M \geqslant 1.2$ and about 15 per cent at $M = 1.0$.

Fig.23 also shows an increase in y_v due to the modification which is less well-defined than that for n_v because of greater scatter in the basic model results. The greatest increase in y_v due to the modification seems to be between $M = 1.0$ and 1.2.

The increase in $m_\theta^\cdot$ seen in Fig.22 for the modified model 6 at $M \leqslant 1.05$ is not substantiated by the results near $M = 1.0$ from model 4. Slender body theory[8] in fact predicts a decrease in $m_\theta^\cdot$ due to the modification and the results from model 6 at $M \leqslant 1.05$ must therefore be accepted with caution; they are nevertheless presented because no reason for the apparent anomaly can be found in the data analysis procedures.

Fig.24 shows a similar unsubstantiated increase in ℓ_p from model 6 at $M \leqslant 1.05$. At $M \geqslant 1.7$ models 4 and 6 (one data point each) indicate a possible decrease in ℓ_p due to the modification but the decreased level is judged to be only marginally outside the general scatter band for this derivative.

For ℓ_v and $(n_r - n_v^\cdot)$, Figs.24 and 25, the present measurements show no changes due to the modification.

There is considerable scatter in the measured manoeuvre margin (Fig.26) largely due to the scatter in z_w (Fig.21) so that the possible rearward shift in aerodynamic centre suggested by the increase in m_w (Fig.21) cannot be substantiated. The theoretical estimates for manoeuvre margin in Fig.26 include thickness effects (equation (B-3)) and are factored by the increases in z_w and m_w suggested by slender body theory.

6 CONCLUSIONS

The longitudinal and lateral dynamic stability of a slender wing/vertical fin configuration has been measured in free flight at Mach numbers from 0.8 to 2.0 and at free-stream Reynolds numbers between 15 and 40 millions per metre.

Two of the test models were of the basic wing plus fin configuration (unmodified models) and two were of this basic configuration fitted with a small fairing which simulated the shroud fitted over the support sting of the complementary wind-tunnel models (modified models). These four models were tested at nominally zero angle of attack. A fifth model of the basic unmodified shape was tested at moderate trimmed lift (lifting model).

Measurements were obtained of the derivatives z_w, m_w, $m_{\dot{\theta}}$, y_v, n_v, ℓ_v, $(n_r - n_{\dot{v}})$, ℓ_p and of the manoeuvre margin. These measurements have been compared with theoretical estimates based on existing, easily-applied methods. Comparisons have also been made between the experimental results to assess the effect of the moderate lift and the effect of the shape modification on the measured derivatives. These comparisons have resulted in the following conclusions:-

(1) Comparison of the nominally zero-lift (unmodified) model results with theoretical estimates is generally good particularly at supersonic speeds. There are, however, two notable exceptions:-

(a) the supersonic variation of m_w shows a greater Mach number dependency than that indicated by linearised theory, and at transonic speeds the measured m_w is considerably greater than indicated by theory;

(b) the experimental pitch damping does not show the marked peak at sonic speed indicated by theory.

(2) Comparison of the lifting model results with those from the non-lifting models reveals that only the derivatives due to sideslip n_v, y_v and ℓ_v and the pitching moment derivative m_w show any measurable variation due to angle of attack. Also these variations were confined largely to transonic speeds, possibly because the angle of attack of the lifting model was small ($\alpha_T \approx 1$ degree) at supersonic speeds. The increment in m_w and ℓ_v at transonic speeds was largely consistent with the estimated increments due to angle of attack, $\Delta m_w = -1.58\alpha_T$ and $\Delta \ell_v = \ell_{vw}\alpha_T$, based on slender theory.

(3) Comparison of the results from the modified models with those from the unmodified basic models at zero lift reveals small but consistent differences in m_w, n_v and y_v that may reasonably be ascribed to the dummy sting fairing. Differences in the derivatives $m_{\dot{\theta}}$ and ℓ_p are less significant and may be due entirely or in part to experimental uncertainties. The remaining derivatives z_w, ℓ_v and $(n_r - n_{\dot{v}})$ appear unaffected by the modification.

Appendix A

EQUATIONS OF MOTION USED IN DIGITAL ANALYSIS

The equations of motion used as the basis of the least-squares fitting technique[4] are listed below, together with the relationships between the accelerations measured with respect to moving and earth-fixed axes.

$$\dot{w} = z_w w\rho SV/m + qV - pv + g \cos\theta \cos\phi$$

$$\dot{q} = m_w w\rho S\bar{c}/I_y + (m_q + m_{\dot{w}})q\rho S\bar{c}^2/I_y + m_t \rho SV^2 s/I_y + b_y pr$$

$$\dot{v} = y_v v\rho SV/m + pw - rV + g \cos\theta \sin\phi$$

$$\dot{p} = \ell_v v\rho SVs/I_x + \ell_p p\rho SVs^2/I_x + \ell_r r\rho SVs^2/I_x + \ell_{vw} vw\rho Ss/I_x + \ell_t \rho V^2 Ss/I_x + b_x qr$$

$$\dot{r} = n_v v\rho SVs/I_z + n_p p\rho SVs^2/I_z + (n_r - n_{\dot{v}})\rho SVs^2/I_x + n_{vw} vw\rho Ss/I_z + n_t \rho V^2 Ss/I_z + b_z pq$$

$$\dot{V} = -\rho SV^2 C_D/2m - g \sin\theta$$

$$\dot{\theta} = -g \cos\theta/V$$

$$\dot{\phi} = p$$

$$\dot{z} = V \sin\theta$$

$$a_y = y_v v\rho SV/m + (pq + \dot{r})x_1 - (p^2 + r^2)y_1 + (qr - \dot{p})z_1$$

$$a_z = z_w w\rho SV/m + (pr - \dot{q})x_1 + (qr + \dot{p})y_1 - (p^2 + q^2)z_1$$

For the model with an incidence probe in the nose, the pressure readings are related to the local angles of attack and sideslip,

$$C_{p_w} = \rho VK_w(w - qx_p)$$

$$C_{p_v} = \rho VK_v(v - rx_p)$$

where K_w and K_v are obtained from the calibration of the probe, and x_p is the distance of the probe from the CG. The probe data may also be used in the least-squares fitting process.

The derivatives ℓ_r and n_p are assumed to be known, and given by the theoretical estimates. The moment equations also contain terms in ℓ_t, m_t, n_t to represent the moments due to the control settings.

Appendix B

ESTIMATION METHODS

B.1 z_w (Fig. 9)

At supersonic speeds estimates of z_w have been obtained from Refs.9 and 10. The charts of Ref.9 are based on linearised theory applied to cropped delta wings at supersonic speeds having subsonic leading edges and streamwise tips which lie entirely upstream of any mutual interference. These conditions are fulfilled by the present 'equivalent' wing for $1.08 < M < 2.3$. In Ref.10 the lift-curve slope has been calculated (in terms of the parameter $\beta s/c_0$) for a 'modified gothic' planform $s(x) = 0.4\ (1.25x - 0.25x^5)$ which differs only trivially from the present real wing planform, the maximum difference in local semi-span being only about 3.6 per cent. The 'not-so-slender' wing theory of Ref.10 should apply to the present wing $(s/c_0 = 0.4)$ up to about $M = 1.3$, when $(\beta s/c_0)^2 = 0.1$.

At subsonic speeds a value of z_w has been calculated using the charts of Ref.19 which are compiled mainly from the experimental results of Ref.20. Wing thickness is incorporated as the ratio of wing frontal area to planform area, S_f/S ; this ratio for the tests of Ref.20 was 0.04 and use was made of a correction factor in Ref.19 to extend the data to $S_f/S = 0.104$ for the present wing (note $S_f/S = t/c$) .

Further estimates for the present (equivalent) wing at subsonic speeds were made using the carpet charts of Ref.11 (basically Multhopp's subsonic lifting-surface theory). Use of these charts entailed some interpolation for taper ratio and this, together with the limitations of small wing-thickness and inviscid flow, makes the estimates from Ref.11 somewhat tentative.

Ref.8 was used to obtain the slender-body value of z_w at $M = 1.0$.

The calculated effect of lift on z_w is based on the expression from slender theory

$$C_L = \left(\frac{\pi A}{2} + 4|\alpha_T|\right)\alpha_T \quad , \tag{B-1}$$

suggested in Ref.9, giving an increment

$$\Delta z_w = -4|\alpha_T| \quad . \tag{B-2}$$

B.2 m_w (Fig.9)

Values of m_w at supersonic speeds for the 'equivalent' cropped delta wing were estimated using the aerodynamic centre position, h, and lift-curve slope, z_w, obtained from the charts of Ref.9; m_w being related to the lift-curve slope by $m_w = (h - h_0)z_w$, where h_0 is the moment-axis position, i.e. the centre-of-gravity position of the model. The same limitations apply as for z_w at supersonic speeds (section B.1) and the estimates are therefore valid only for $M > 1.08$.

At transonic speeds ($M = 1$ to 1.3) the 'not-so-slender' wing theory of Ref.10 was used to obtain both the aerodynamic centre position and lift-curve slope and hence m_w, for the 'modified gothic' planform (section B.1).

At subsonic speeds m_w was calculated from the data of Refs.11 and 19. The empirical data of Ref.19 refer to delta wings having a thickness/chord ratio of 4 per cent compared with 10.4 per cent for the present wing. A tentative correction for this difference in thickness has been obtained from the tests of Ref.21 which indicate that the centre of *linear* lift (at $C_L \approx 0$) moves forward with increasing thickness by about 2 per cent of the centre-line chord over the thickness range 4 per cent $\leqslant t/c \leqslant$ 10 per cent. This represents a destabilizing increment in m_w of about 0.022 for the present wing. It is emphasised that the tests of Ref.21 were conducted at low speed ($M \approx 0.2$) and at a Reynolds number of 2.24 millions based on centre-line chord compared with 23.0 millions for the present test associated with $M = 0.9$, i.e. the lowest speed at which m_w was measured.

The estimates from Ref.11 refer to the 'equivalent' cropped delta wing and are subject to the same limitations already given in section B.1 for z_w, i.e. they are restricted to thin wings and inviscid flow.

Thickness effects in m_w have been applied to the thin-wing estimates of Ref.9 (supersonic), Ref.10 (transonic) and Ref.11 (subsonic) using the integral expression based on slender body theory given in Ref.1,

$$\Delta\bar{x} = \int_0^1 \frac{s^2(x)}{s^2} \left[1 - 4\left(\frac{r_0}{s(x)}\right)^2 \left(1 - \frac{2\theta}{\pi}\right) + \frac{2}{\pi}\tan\theta\right] dx \quad . \qquad \text{(B-3)}$$

The required conformal transformation for wings with diamond shaped cross-sections has been obtained by E.C. Maskell in some unpublished RAE work as:

$$\frac{r_0}{s(x)} = c_0 \pi^{\frac{1}{2}} / 2 \cos \theta \Gamma\left(1 - \frac{\theta}{\pi}\right) \Gamma\left(\tfrac{1}{2} + \frac{\theta}{\pi}\right) , \qquad \text{(B-4)}$$

where $2\theta(x)$ is the total angle of the diamond cross-section normal to the longitudinal axis. Equation (B-3) gives the rearward shift in aerodynamic centre as a fraction of centre-line chord; Δm_w then follows from $\Delta \bar{x} c_0 z_w / \bar{c}$.

The effect of lift on m_w is calculated on the assumption that the slender theory value of 4 per cent c_0 shift in centre of pressure between $C_L = 0$ and $C_L = 0.1$ given in Ref.9 is valid for the present 'equivalent' wing. This assumption results in the relationship:

$$m_w(\text{lift}) = m_{w_0} - 1.58 \, |\alpha_T| , \qquad \text{(B-5)}$$

where m_{w_0} is the value of m_w at zero lift.

B.3 $m_{\dot{\theta}}$ $(= m_q + m_{\dot{w}})$ (Fig.10)

Component derivatives of pitch damping, m_q and $m_{\dot{w}}$, were obtained for the equivalent cropped delta wing at supersonic speeds from Refs.14 and 15 respectively. The basis for the estimates of m_q in Ref.14 is supersonic linearised theory and that for $m_{\dot{w}}$ in Ref.15 is the linearised time-dependent wave equations for wings in accelerated motion as reported in Refs.22 and 23. These data are applicable to a wing with subsonic leading edges, supersonic trailing edges and for conditions where the inboard Mach lines from the cropped delta wing tip leading edges cannot intersect on the wing. These conditions are met for the present (equivalent) wing for $1.075 \leqslant M \leqslant 2.3$.

At sonic speeds slender body theory (e.g. Ref.8) gives $m_{\dot{\theta}} = -(c_0 - h_0/\bar{c})^2 \pi A/4$ which, for the present (actual) wing planform, gives $m_{\dot{\theta}} = -0.815$.

At subsonic speeds $m_{\dot{\theta}}$ was estimated from Ref.12 based on an extension of Multhopp's subsonic lifting-surface theory[13].

For evaluating the effect of angle of attack on $m_{\dot{\theta}}$, Garner and Lehrian[24] have estimated the effects of leading edge separation on the pitching derivatives of a gothic wing which leads to the expression:

$$m_{\dot{\theta}(\text{lift})} = m_{\dot{\theta}_{\alpha_T=0}} - 0.17\alpha_T . \qquad \text{(B-6)}$$

B.4 y_v (Fig.11)

The wing contribution to y_v is considered negligibly small for the basic shape models. Slender body theory gives zero side force due to the body, this being dependent only on the cross-sectional area at the trailing edge.

For the fin contribution;

$$y_{v_R} = -\tfrac{1}{2}S_F/S \times \text{lift-curve slope} \quad , \tag{B-7}$$

was used where the lift-curve slope was obtained for supersonic speeds from Ref.9 using the cropped delta equivalent fin planform and considering the wing to be a complete reflection plate for the fin. Ref.9 was applicable only up to $M = 1.68$ when the fin leading-edge ceased to be subsonic.

Between $M = 1$ and 1.2 the lift-curve slope was obtained using the 'not-so-slender' theory of Ref.10 for the 'modified gothic' planform.

At $M = 1$ the sonic theory value of $\pi A/2$ for lift-curve slope is appropriate.

For subsonic speeds the lift-curve slope was obtained from Ref.11 taking again the equivalent cropped delta planform for the fin plus its total reflection.

Wing-fin interference was corrected for by a factor, k, derived from Ref.25 and applied such that

$$y_{v_F} = k y_{v_R} \quad . \tag{B-8}$$

$$\text{The factor } k = \left[\frac{y_{v_{W+F}} - y_{v_W}}{y_{v_R}}\right] \quad . \tag{B-9}$$

where the terms inside the brackets, evaluated by slender body theory, are the side force of the wing-plus-fin, of the wing alone and of the fin-plus-reflection alone. For $M < 1.68$ the leading edge of the fin is subsonic and the factor k may be regarded as constant.

B.5 n_v (Fig.11)

The wing contribution to n_v arising out of the thickness distribution was calculated from the integral expression of Ref.26:

$$n_{v_W} = 4A\left(\frac{c_0}{b}\right)^3 \int_0^1 \left[\left(\frac{s_L}{c_0}\right)^2 \tan\theta - 4\left(\frac{r_0}{c_0}\right)^2 \theta\right] d\left(\frac{x}{c_0}\right) \quad , \tag{B-10}$$

where r_0 = radius of transformed circle, and

$$\frac{r_0}{c_0} = \left(\frac{s_L}{c_0}\right) \frac{\pi^{\frac{1}{2}}}{2} \frac{\sec\theta}{\Gamma\left(1 - \frac{\theta}{\pi}\right)\Gamma\left(\frac{1}{2} + \frac{\theta}{\pi}\right)} \quad , \tag{B-4}$$

where $\theta(x)$ is the leading-edge semi angle of the cross section.

The fin contribution was calculated from

$$n_{v_R} = -(X_F/s)y_{v_R} \quad , \tag{B-11}$$

for the 'equivalent' cropped delta fin plus its reflection, where s is the semi-span of the wing at the trailing edge and X_F is the distance of the aerodynamic centre of the fin behind the centre-of-gravity position of the model; the fin aerodynamic centre was obtained for the reflected fin from Ref.9 at supersonic speeds and from Ref.11 at subsonic speeds.

A correction factor for wing-fin interference, evaluated from the analogous form of equation (B-9) was applied as a constant over the speed range of the tests.

The effect of angle-of-attack on n_v has been neglected.

B.6 ℓ_v (Fig.12)

The direct fin contribution to ℓ_v (curve A Fig.12) is composed of the product of the side force due to sideslip, y_{v_R}, and the fin moment arm above the wing; the latter, from slender body theory, being $4s_F/3\pi$ gives a rolling moment

$$\ell_{v_R} = \frac{4}{3\pi}\left(\frac{s_F}{s}\right) y_{v_R} \quad . \tag{B-12}$$

The direct fin contribution to ℓ_v is opposed by a rolling moment due to the pressure field on the wing surface induced by the presence of the sideslipping fin. At supersonic speeds this fin-wing interference pressure field is confined to the wing surface downstream of the sonic line from the fin root leading edge. Theoretical estimates of this interference effect have been made

in Ref.16 for a triangular vertical fin surface in the presence of a symmetrical triangular horizontal tail surface (curve B, Fig.12). The conditions of applicability of Ref.16 are restricted to subsonic leading edges of both surfaces and to speeds where the sonic lines from the root leading edge of the vertical fin intersect the trailing edge of the horizontal (wing) surface - these conditions apply for the present configuration for $1.3 < M < 1.68$.

At sonic speed, slender body theory is used to develop an algebraic expression[18] for ℓ_v due to the fin plus wing.

The increment in ℓ_v due to angle of attack, $\Delta\ell_v = \ell_{vw}\alpha_T$, was derived from slender wing theory where the rolling moment due to combined sideslip and angle of attack, ℓ_{vw} , is the estimated value from Ref.17.

B.7 ℓ_p (Fig.12)

The wing contribution to roll damping, ℓ_{p_W} , was obtained for supersonic speeds from Refs.27 and 28 based on linearised supersonic flow theory. At $M = 1$ the sonic theory value of $\ell_{p_W} = -\pi A/32$ was used.

For subsonic speeds the charts of Ref.29, based on Weissinger's simplified lifting-surface theory, were used.

The fin contribution to roll damping, ℓ_{p_R} , was obtained from the expression,

$$\ell_{p_R} = -\frac{3}{2\pi}\frac{2A_R}{3}(s_F/s)^2\frac{S_F}{S} \quad . \tag{B-13}$$

This expression is based on slender body theory as derived in Ref.1, where A_R is the aspect ratio of the fin-plus-reflection.

Wing-fin interference is assumed confined to the effect of sidewash on the fin induced by the loading on the wing; this reduces the effectiveness of the fin.

As in Ref.1, an average value of sidewash angle (σ) over the fin height was used as evaluated in Ref.26 *viz.*

$$\left(\frac{\partial\sigma}{\partial\left(\frac{pb}{2V}\right)}\right)_{aV} = \frac{s_L}{b}\left[\left(1+\frac{s_{F_L}^2}{s_L^2}\right)^{\frac{1}{2}} - \frac{s_{F_L}}{s_L}\right] \quad , \tag{B-14}$$

where $\frac{pb}{2V}$ is the wing-tip helix angle and where s_L is the local semispan

of the wing and s_{F_L} is the local height of the fin, both measured at the chordwise position of the centre of pressure of the fin.

The total roll-damping derivative due to the fin is thus,

$$\ell_{p_F} = \left\{1 - \left[\frac{\partial\sigma}{\partial\left(\frac{pb}{2V}\right)}\right]_{aV}\right\}\ell_{p_R} \quad . \tag{B-15}$$

Equations (B-13) to (B-15) give for the present configuration $\ell_{p_F} = -0.007$.

The total roll damping derivative for the complete configuration is thus,

$$\ell_p = \ell_{p_W} + \ell_{p_F} \quad .$$

B.8 $(n_r - n_{\dot{v}})$ (Fig.13)

Although slender-body theory gives a non-zero value for n_r alone, the oscillatory damping $n_r - n_{\dot{v}}$ is zero, being dependent on the cross-section shape at the trailing edge only.

For the fin contribution, the fin plus reflection may be considered as a cropped delta wing and the same methods[14,15] may be used to evaluate n_r and $n_{\dot{v}}$ as used for the analogous longitudinal derivatives m_q and $m_{\dot{w}}$. The conversion to wing representative length and area is given by

$$(n_r - n_{\dot{v}})_R = \left(\frac{\bar{c}_F}{s}\right)^2 \frac{S_F}{S}(m_q + m_{\dot{w}}) \quad . \tag{B-16}$$

An alternative method of estimation used in Ref.1 and based on Ref.30, applicable to zero angle of attack, is

$$(n_r - n_{\dot{v}})_R = \left(\frac{X_F}{s}\right)^2 y_{v_R} \quad . \tag{B-17}$$

A correction factor for wing-fin interference effects was derived from slender body theory[8]; this factor is equal to that for y_v (section B.4) since the oscillatory yaw damping is also dependent only on the configuration at the trailing edge.

Table 1

MODEL DATA

Wing

Area	0.955 m^2
Aspect ratio	1.385
Span/length ratio	0.8
Geometric mean chord	0.8305 m
Centre-line chord	1.437 m
Span	1.15 m
Volume	0.0488 m^3
Thickness/chord ratio on centre line	0.104
Newby area distribution	4 stx(c_0 - x)
Zero camber and twist	

Fin

Area (gross)	0.0955 m^2
Aspect ratio (gross)	1.077
Geometric mean chord	0.298 m
Centre-line chord	0.515 m
Height	0.32 m

Elevators (model 3 only)

Area	2 × 0.025 m^2
Chord	0.1 m
Span	0.25 m each
Inboard edge	0.068 m from centre line of wing

Port elevator set at 5.5 degrees
Starboard elevator set at 4.5 degrees

Mass

Model 1	133.83 kg
Model 3	141.7 kg
Model 4	140.9 kg
Model 5	142.2 kg
Model 6	141.6 kg

Inertia

Model	1	3	4	5	6
Inertia in roll, Ix	3.77	3.99	3.9	3.97	3.68
Inertia in pitch, Iy	14.75	15.3	14.64	14.96	15.28
Inertia in yaw, Iz	18.18	18.97	18.18	18.66	18.56
Product of inertia Ixz	-0.176	-0.09	-0.19	-0.15	-0.07

kg m^2

Centre of gravity of all models was at $\frac{1}{2}c_0$.

Table 2 - NOTATION FOR STABILITY DERIVATIVES

Present report		Ref. 32	
Symbol	Definition*	Symbol	Relationship**
ℓ_p	$L_p/\rho VSs^2$	$\breve{L}_p$	$\frac{2s^2}{\ell_2^2}\ell_p$
ℓ_r	$L_r/\rho VSs^2$	$\breve{L}_r$	$\frac{2s^2}{\ell_2^2}\ell_r$
ℓ_v	$L_v/\rho VSs$	$\breve{L}_v$	$\frac{2s}{\ell_2}\ell_v$
m_q	$M_q/\rho VS\bar{c}^2$	$\breve{M}_q$	$\frac{2\bar{c}^2}{\ell_1^2}m_q$
$m_{\dot{w}}$	$M_{\dot{w}}/\rho S\bar{c}^2$	$\breve{M}_{\dot{w}}$	$\frac{2\bar{c}^2}{\ell_1^2}m_{\dot{w}}$
m_w	$M_w/\rho VS\bar{c}$	$\breve{M}_w$	$\frac{2\bar{c}}{\ell_1}m_w$
n_p	$N_p/\rho VSs^2$	$\breve{N}_p$	$\frac{2s^2}{\ell_2^2}n_p$
n_r	$N_r/\rho VSs^2$	$\breve{N}_r$	$\frac{2s^2}{\ell_2^2}n_r$
$n_{\dot{v}}$	$N_{\dot{v}}/\rho Ss^2$	$\breve{N}_{\dot{v}}$	$\frac{2s^2}{\ell_2^2}n_{\dot{v}}$
n_v	$N_v/\rho VSs$	$\breve{N}_v$	$\frac{2s}{\ell_2}n_v$
y_v	$Y_v/\rho VS$	$\breve{Y}_v$	$2y_v$
z_w	$Z_w/\rho VS$	$\breve{Z}_w$	$2z_w$

* Definitions of basic symbols are given in the list of symbols

** ℓ_1 and ℓ_2 are the representative lengths for the longitudinal and lateral stability derivatives, respectively

Symbols

A	aspect ratio
a_y, a_z	components of acceleration
b	wing span at trailing edge
C_D	drag coefficient, $\text{Drag}/\frac{1}{2}\rho V^2 S$
c_0	wing centre-line chord
b_x, b_y, b_z	inertia ratios, $b_x = (I_z - I_y)/I_x$ etc
C_F	root chord of fin (Fig.1)
$\bar{c}$	wing geometric mean chord
$\bar{c}_F$	fin geometric mean chord
C_L	lift coefficient = $\text{Lift}/\frac{1}{2}\rho V^2 S$
g	acceleration due to gravity
h	position of aerodynamic centre of wing, aft of apex
h_0	position of moment axis (centre of gravity) aft of wing apex
I_x, I_y, I_z	moments of inertia in roll, pitch and yaw, respectively
I_{xz}	product of inertia
k	interference factor, defined in equation (B-9)
$\mathcal{L}$	rolling moment
L_p, L_r, L_v	rolling moment derivatives, eg $L_v = \partial\mathcal{L}/\partial v$
ℓ_p, ℓ_r, ℓ_v,	see Table 2
ℓ_t	rolling moment coefficient associated with trim
ℓ_{vw}	$d\ell_v/d\alpha$, per radian
M	free-stream Mach number
$\mathcal{M}$	pitching moment
M_q, M_w, $M_{\dot{w}}$	pitching moment derivatives, eg $M_q = \partial\mathcal{M}/\partial q$
m	mass of model
m_q, m_w, $m_{\dot{w}}$	see Table 2
m_t	pitching moment coefficient associated with trim
$m_{\dot{\theta}}$	$m_q + m_{\dot{w}}$
$\mathcal{N}$	yawing moment
N_p, N_r, N_v, $N_{\dot{r}}$	yawing moment derivatives, e.g. $N_v = \partial\mathcal{N}/\partial v$
n_p, n_r, n_v, $n_{\dot{v}}$	see Table 2
n_t	yawing moment coefficient associated with trim
p, q, r	rates of roll, pitch and yaw respectively
r_0	radius of transformed circle corresponding to wing cross section, equation (B-4)
S	wing planform area
S_F	fin planform area (gross)

Symbols (continued)

S_f	maximum projected frontal area of wing
s	semispan of wing at trailing edge
s_L	local semispan of wing
s_F	height of fin at trailing edge
s_{FL}	local height of fin
$s(x)$	local semispan of wing ($c_0 = 1.0$)
t/c	thickness/chord ratio of wing
V	velocity along flight path
v	lateral perturbation velocity
w	normal perturbation velocity
X_F	distance of aerodynamic centre of fin from centre of gravity of model
x	distance from wing apex (Fig.1)
x, y, z	body-fixed axes with origin at cg; x positive forward
x_1, y_1, z_1	coordinates of position of accelerometer
x_F	distance from fin apex (Fig.1)
Y	side force
Y_v	side force derivative, due to sideslip, = $\partial Y/\partial v$
y_v	see Table 2
Z	normal force
Z_w	normal force derivative, due to normal velocity = $\partial Z/\partial w$
z_w	see Table 2
α	angle of attack, $\approx w/V$
β	$(M^2 - 1)^{\frac{1}{2}}$
ε	wing apex angle (Fig.1)
ε_F	fin apex angle (Fig.1)
$\theta(x)$	semi-angle of wing cross section at leading edge
θ	flight path angle to horizontal (Appendix A)
Λ_0	angle of wing leading edge sweepback
ρ	air density
σ	sidewash angle = v/V
ϕ	angle of bank

Suffixes

av	average value
F	for the fin alone
R	for the reflected fin

Symbols (concluded)

T	trimmed conditions
W	for the wing alone
W+F	for the wing plus fin

REFERENCES

No.	Author	Title, etc.
1	K.J. Turner A. Jean Ross Geraldine Earley	The dynamic stability derivatives of a slender wing, a comparison of theory with free-flight model tests at near-zero lift, M = 0.8 to 2.4. ARC CP 995 (1966)
2	A. Jean Ross Geraldine F. Edwards A.P. Waterfall	The dynamic stability derivatives of a slender wing at zero and moderate lift, a comparison of theory with free-flight model tests (M = 0.8 to 2.0). ARC CP 1310 (1973)
3	J.A. Hamilton P.A. Hufton	Free-flight techniques for high-speed aerodynamic research. Jour. Roy. Aero. Soc., March, 1956
4	A.P. Waterfall	A technique for the automatic digital analysis of flight dynamic response data. ARC R&M 3699 (1970)
5	A.P. Waterfall	An improved technique of stability testing in free flight at transonic speeds, applied to a non-lifting slender wing. ARC CP 1174 (1969)
6	F.H. Irvine	Notes on some VHF and UHF aerials for use on free-flight rocket-boosted models and guided missiles. RAE Technical Report 72165 (ARC 34336) (1972)
7	D.M. Ridland Patricia Willatts	Measurement of the moments and products of inertia of free-flight dynamic models. RAE Technical Report 71180 (ARC 33860) (1971)
8	A.H. Sacks	Aerodynamic forces, moments and stability derivatives for slender bodies of general cross-section. NACA Tech. Note 3283 (1954)
9	J.H.B. Smith J.A. Beasley A. Stevens	Calculations of the lift slope and aerodynamic centre of cropped delta wings at supersonic speeds. ARC CP 562 (1960)

REFERENCES (continued)

No.	Author	Title, etc.
10	L.C. Squire	Some applications of 'not-so-slender' wing theory to wings with curved leading edges. ARC R&M 3278 (1960)
11	-	Lift-curve slope and aerodynamic centre position of wings in inviscid subsonic flow. Engineering Science Data Item 70011
12	H.C. Garner	Multhopp's subsonic lifting-surface theory of wings in slow pitching oscillations. ARC R&M 2885 (1952)
13	H. Multhopp	Methods for calculating the lift distribution of wings. (Subsonic lifting-surface theory) ARC R&M 2884 (1950)
14	F.S. Malvestuto D.M. Hoover	Lift and pitching derivatives of thin sweptback tapered wings with streamwise tips and subsonic leading edges at supersonic speeds. NACA Tech. Note 2294, (1951)
15	F.S. Malvestuto D.M. Hoover	Supersonic lift and pitching moment of thin sweptback tapered wings produced by constant vertical acceleration. Subsonic leading edges and supersonic trailing edges NACA Tech. Note 2315 (1951)
16	F.S. Malvestuto	Theoretical supersonic force and moment coefficients on a sideslipping vertical - and horizontal-tail combination with subsonic leading edges and supersonic trailing edges NACA TN 3071 (1954)
17	H.S. Ribner F.S. Malvestuto	Stability derivatives of triangular wings at supersonic speeds. NACA Tech. Note 1572 (1948)
18	C.C.L. Sells	Calculation of sideslip derivatives and pressure distribution in asymmetric flight conditions on a slender wing-fin configuration. RAE Technical Note Aero 2805 (ARC 23788) (1962)

REFERENCES (continued)

No.	Author	Title, etc.
19	-	Low-speed longitudinal aerodynamic characteristics of slender wings. Engineering Sciences Data Item 71006
20	D.A. Kirby	An experimental investigation of the effect of planform shape on the subsonic longitudinal stability characteristics of slender wings. ARC R&M 3568 (1967)
21	D.A. Kirby D.L.I. Kirkpatrick	An experimental investigation of the effect of thickness on the subsonic longitudinal stability characteristics of delta wings of 70 degrees sweep-back. ARC R&M 3673 (1969)
22	C. Gardner	Time-dependent linearised supersonic flow past planar wings. Communications on Pure and Appl. Mathematics, Vol. III, No. 1, pp. 33-38 March (1950)
23	C.E. Watkins	Effect of aspect ratio on undamped torsional oscillations of a thin rectangular wing in supersonic flow. NACA TN 1895 (1949)
24	H.C. Garner D.E. Lehrian	Pitching derivatives for a gothic wing oscillating about a mean incidence. ARC CP 695 (1963)
25	F.K. Goodwin G.E. Kaattari	Estimation of directional stability derivatives at small angles and subsonic and supersonic speeds. NASA TIL 6338 (1958)
26	A. Jean Ross	The calculation of lateral stability derivatives of slender wings at incidence, including fin effectiveness, and correlation with experiment. ARC R&M 3402 (1961)

REFERENCES (concluded)

No.	Author	Title, etc.
27	F.S. Malvestuto K. Margolis H.S. Ribner	Theoretical lift and damping-in-roll at supersonic speeds of thin sweptback tapered wings with streamwise tips, subsonic leading edges and supersonic trailing edges. NACA Report 970 (1950)
28	-	Data sheets. Aerodynamics, Aircraft S.06.03.01, Roy. Aero. Soc.
29	-	Data sheets. Aerodynamics, Aircraft 06.01.01, Roy. Aero. Soc.
30	L.R. Fisher H.S. Fletcher	Effect of lag of sidewash on the vertical-tail contribution to oscillatory damping in yaw of airplane models. NACA Tech. Note 3356 (1955)
31	H.S. Ribner	The stability derivatives of low-aspect-ratio triangular wings at subsonic and supersonic speeds. NACA tech. Note 1423 (1947)
32	H.R. Hopkin	A scheme of notation and nomenclature for aircraft dynamics and associated aerodynamics. ARC R&M 3562 Parts 1 to 5 (1966)
33	G. Ehn T. Landén	Measurements of dynamic stability derivatives of Viking model in FFA windtunnel S4 at transonic and supersonic speeds. Flygtekniska Försöksanstalten Status Report AU-925 No. 1

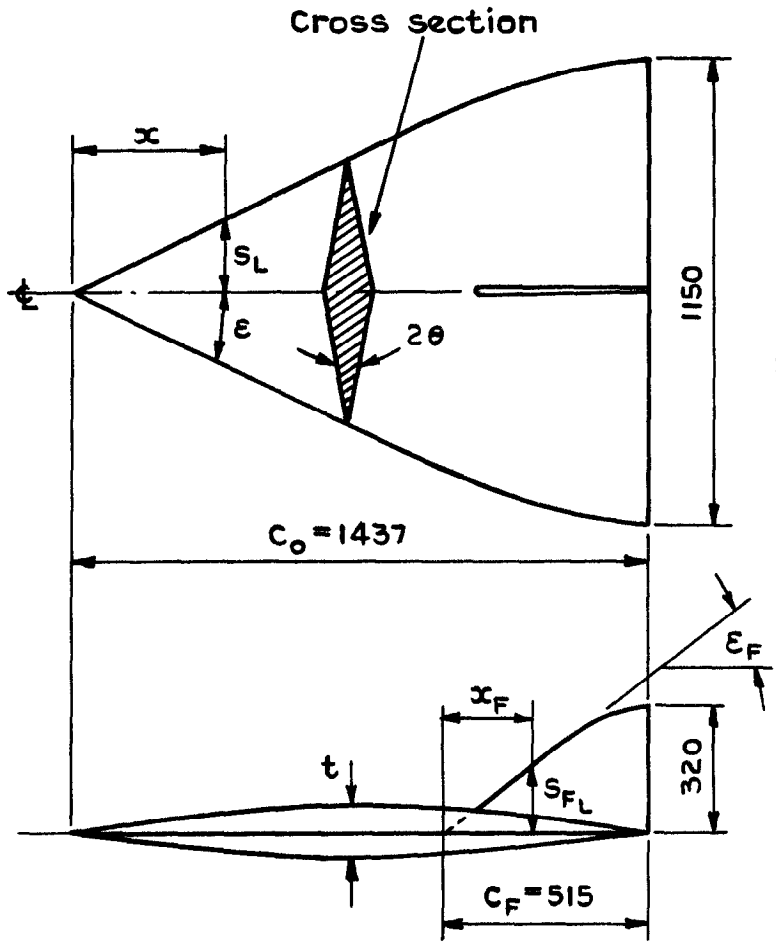

Wing planform

$\tan \varepsilon = 0{\cdot}48$

$S_L = 0{\cdot}48\,x$ for $0 \leq \frac{x}{C_o} \leq \frac{2}{3}$

$S_L = 0{\cdot}48\left[x - \frac{3}{2} C_o \left(\frac{x}{C_o} - \frac{2}{3}\right)^2\right]$

for $\frac{2}{3} \leq \frac{x}{C_o} \leq 1$

Body thickness along ℄

$t = 0{\cdot}416\,x\left(1 - \frac{x}{C_o}\right)$

max $\frac{t}{C_o} = 0{\cdot}104$ at $x = \frac{1}{2} C_o$

Fin planform

$\tan \varepsilon_F = 0{\cdot}7456$

$S_{F_L} = 0{\cdot}7456\,x_F$ for $0 \leq \frac{x_F}{C_F} \leq \frac{2}{3}$

$S_{F_L} = 0{\cdot}7456\left[x_F - \frac{3}{2} C_F \left(\frac{x_F}{C_F}\right) - \frac{2}{3}\right]^2$

for $\frac{2}{3} \leq \frac{x_F}{C_F} \leq 1$

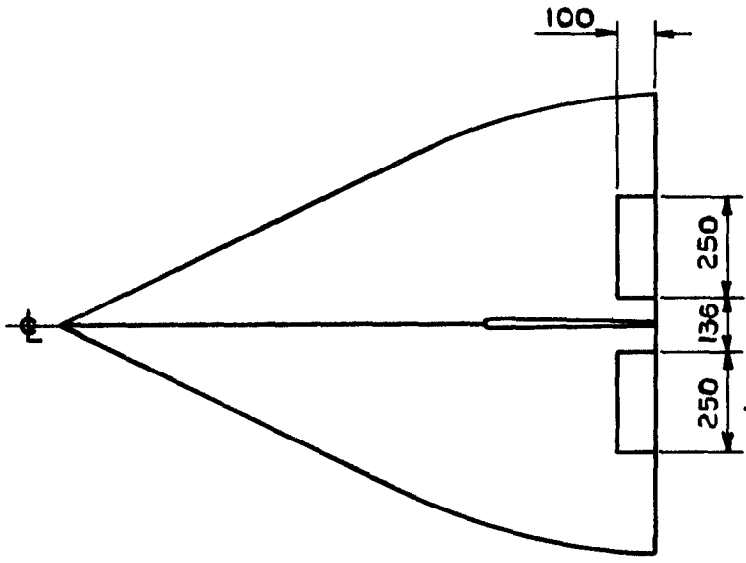

Details of elevators for test of basic shape at lift (model 3)

(Dimensions mm)

Fig.1 Basic shape (models 1, 3 and 5)

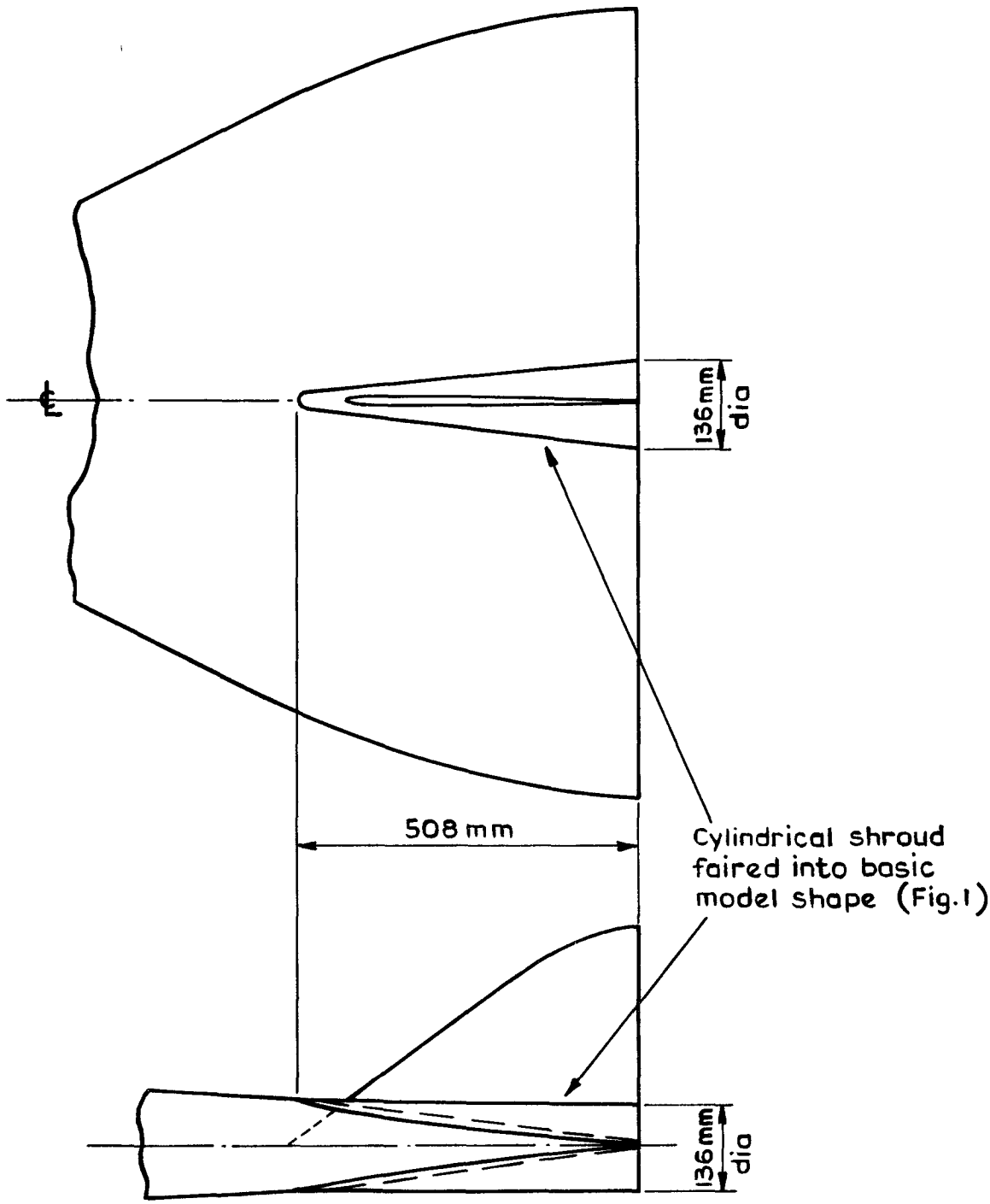

Fig.2 Modified shape (models 4 & 6)

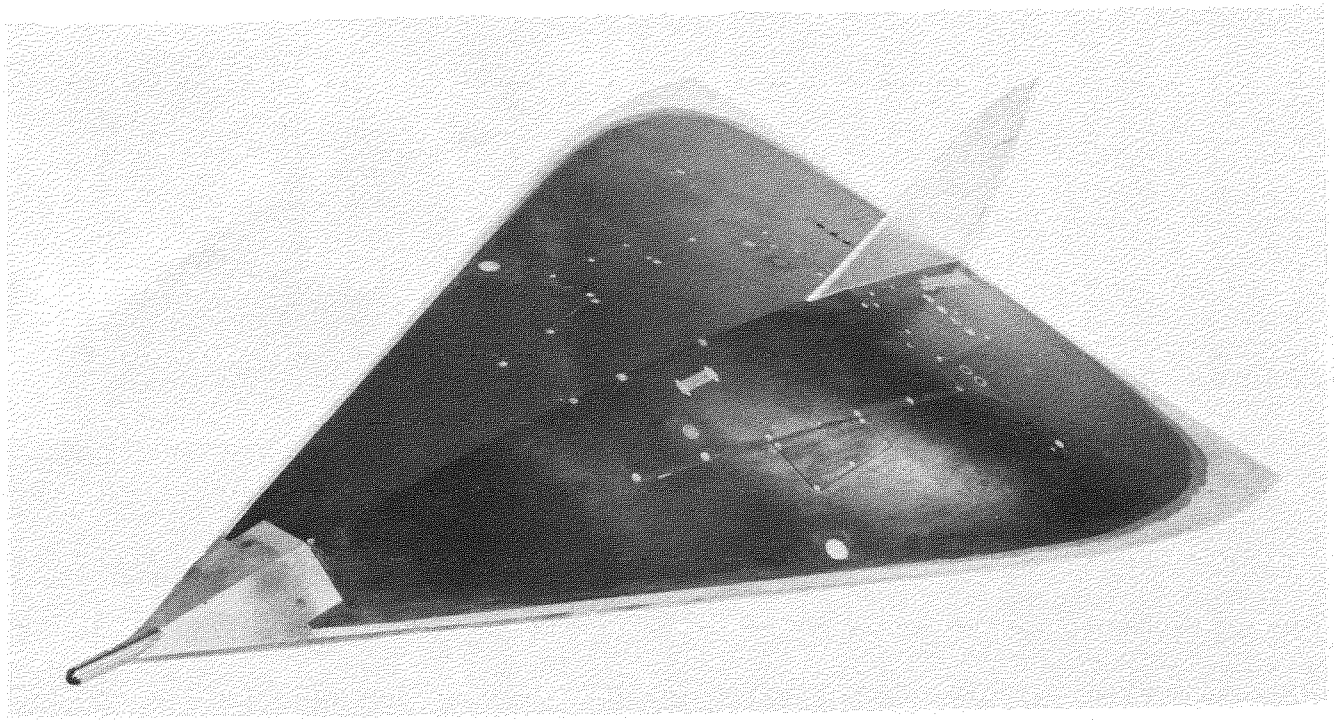

Basic model (1, 3, 5)

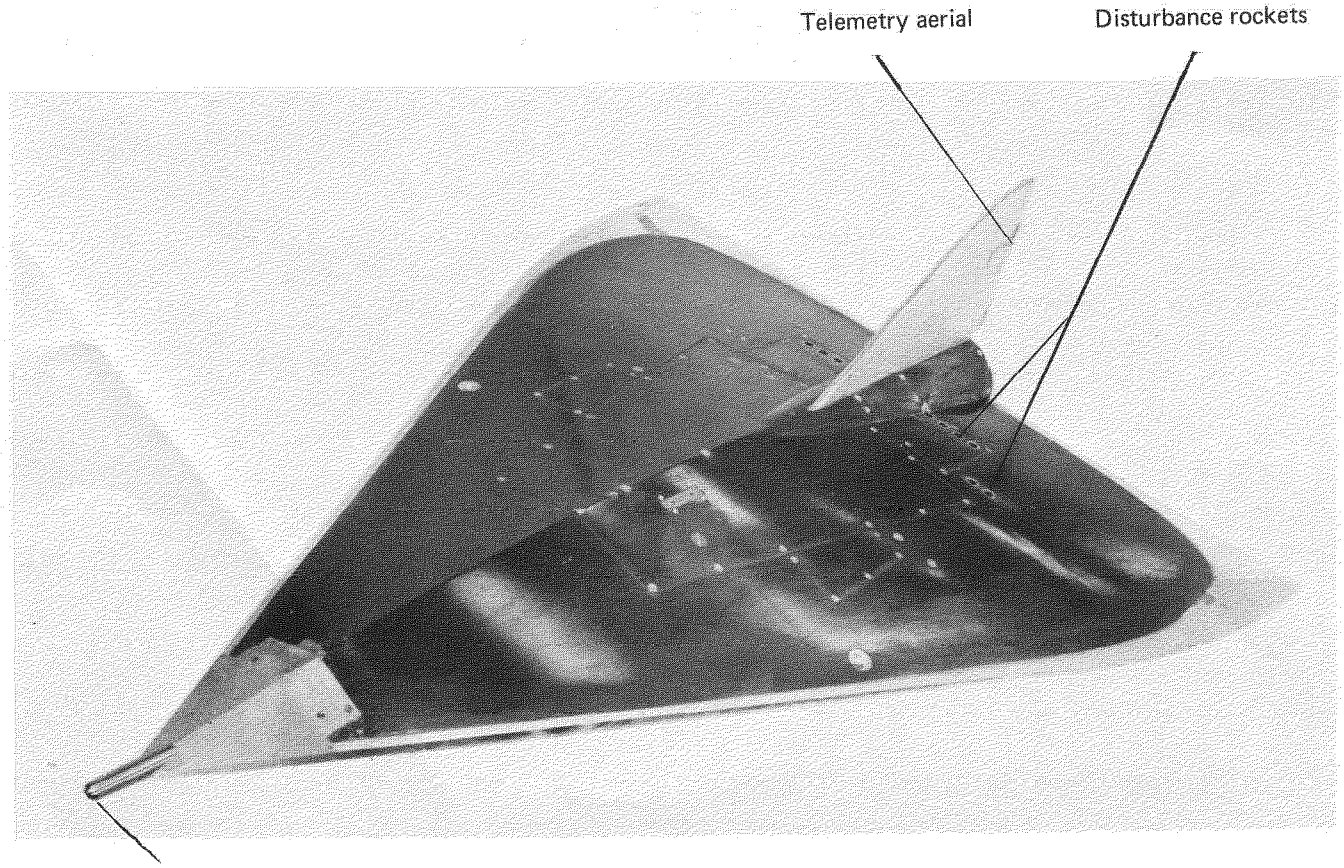

Modified model (4, 6)

Fig.3 Basic and modified models

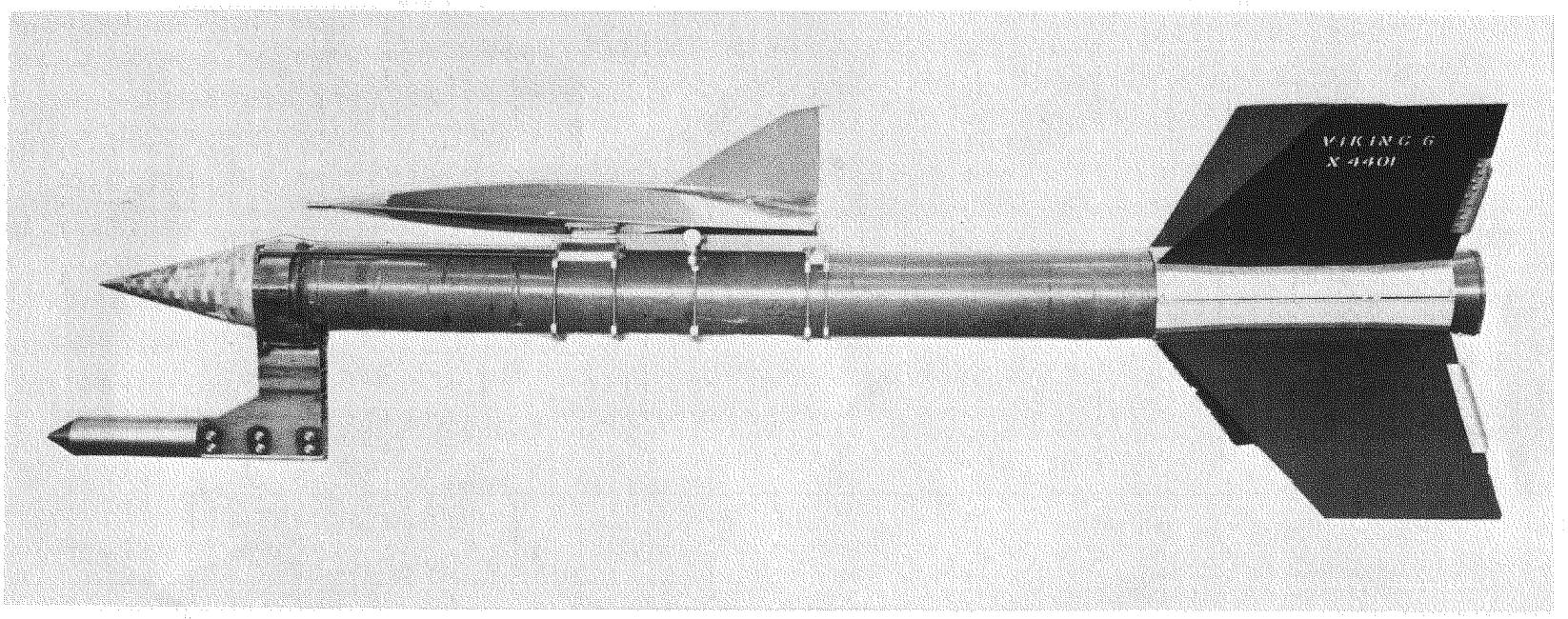

Fig.4 Method of launch

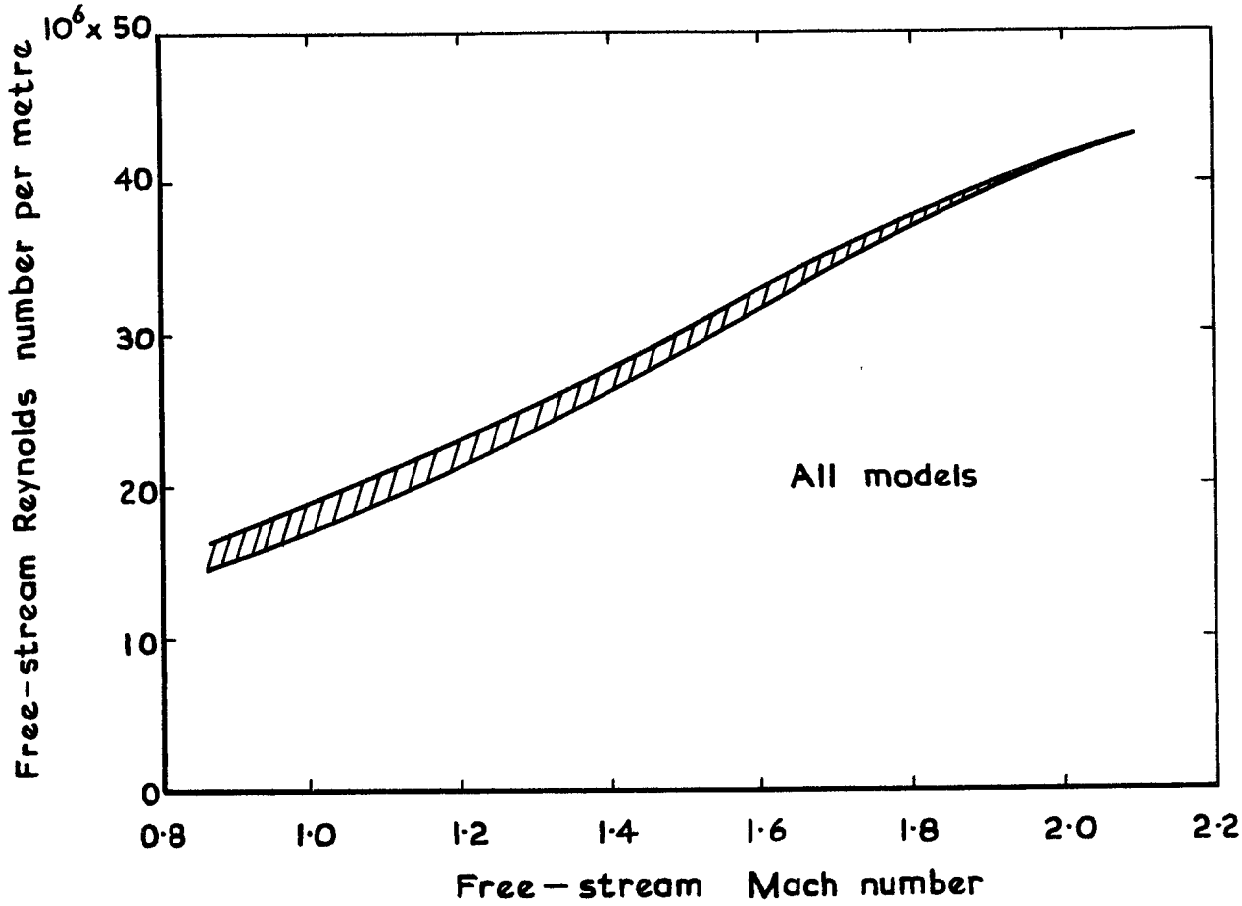

Fig. 5 Reynolds number of tests

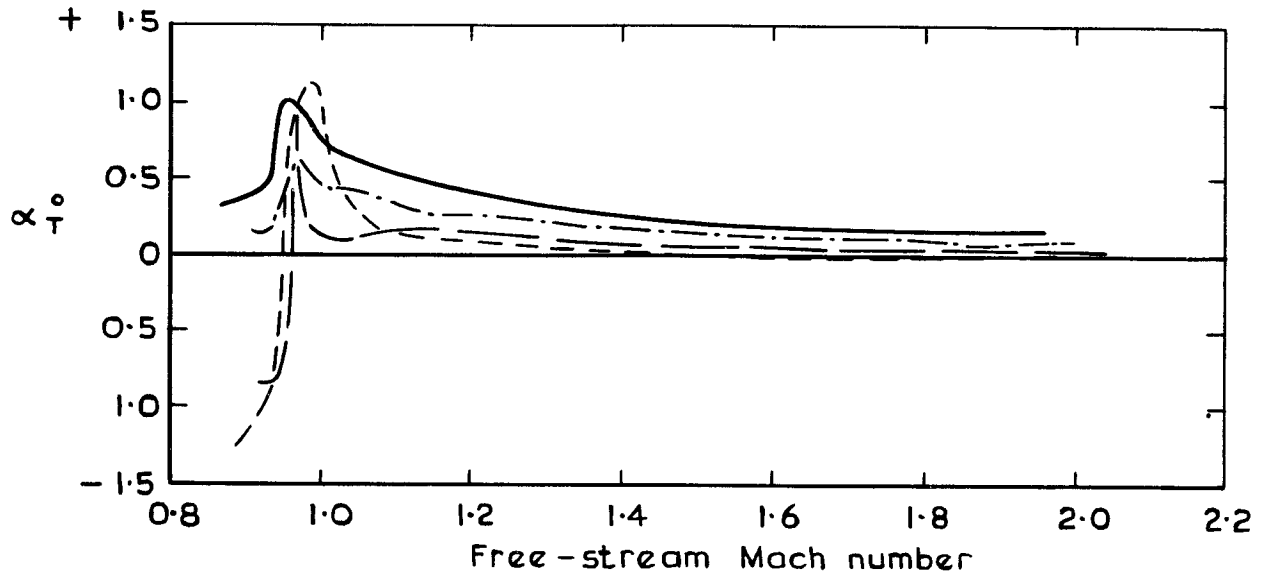

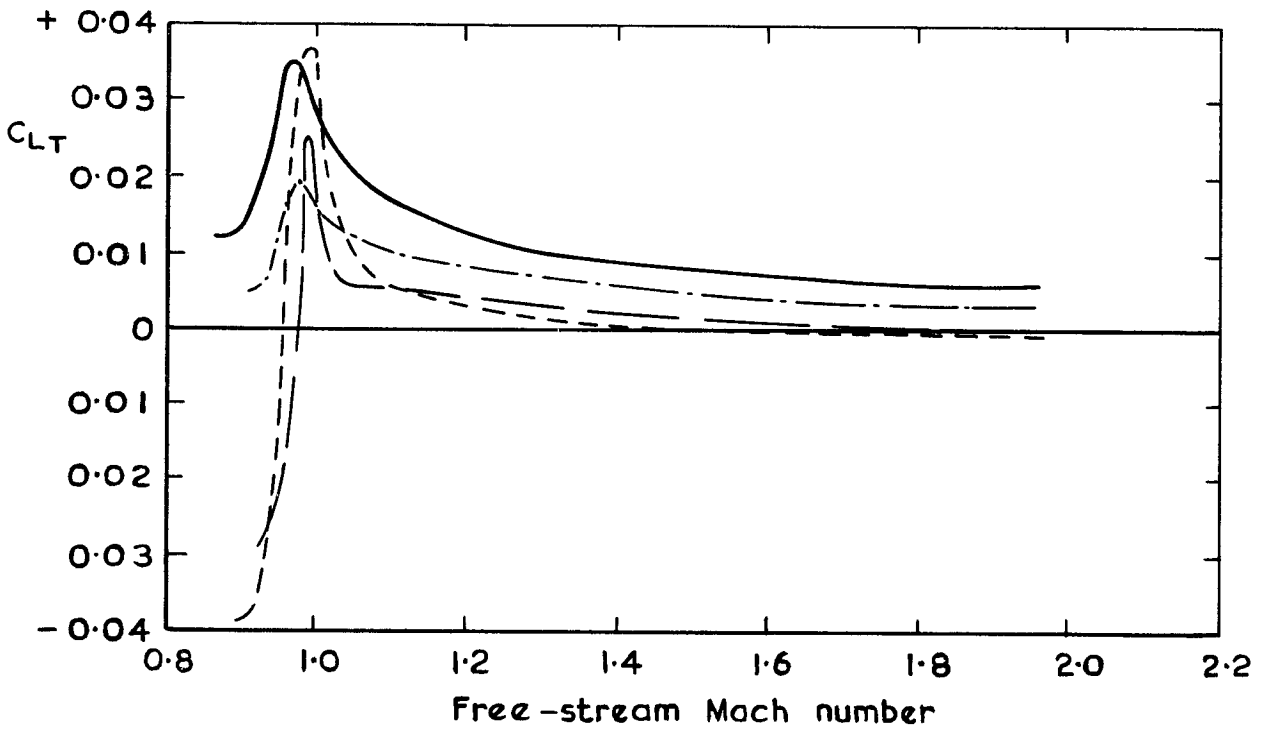

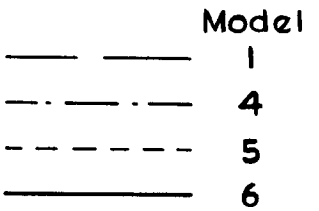

Fig.6 Trimmed conditions—zero-lift models

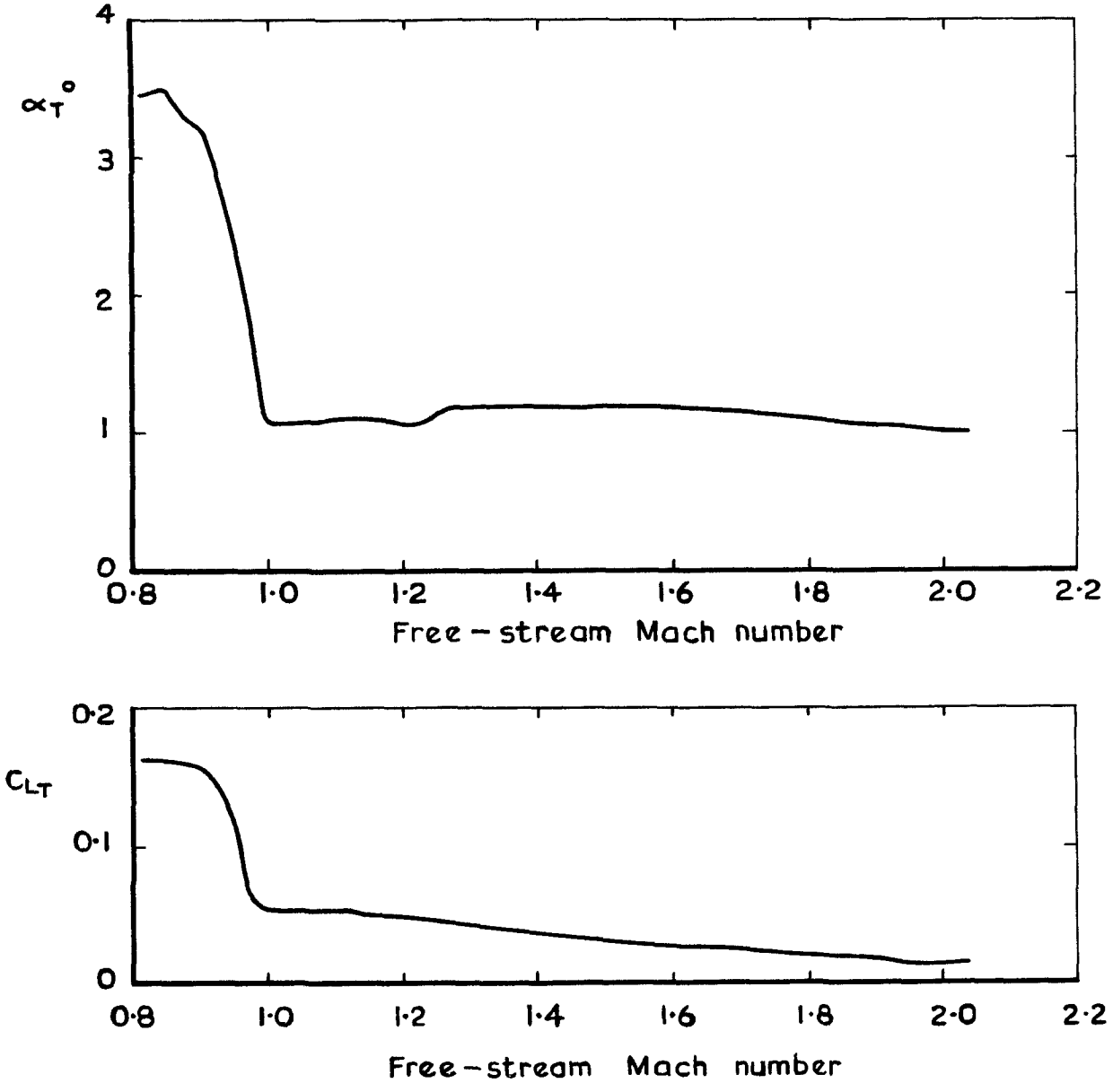

Fig. 7 Trimmed conditions — lifting model (3)

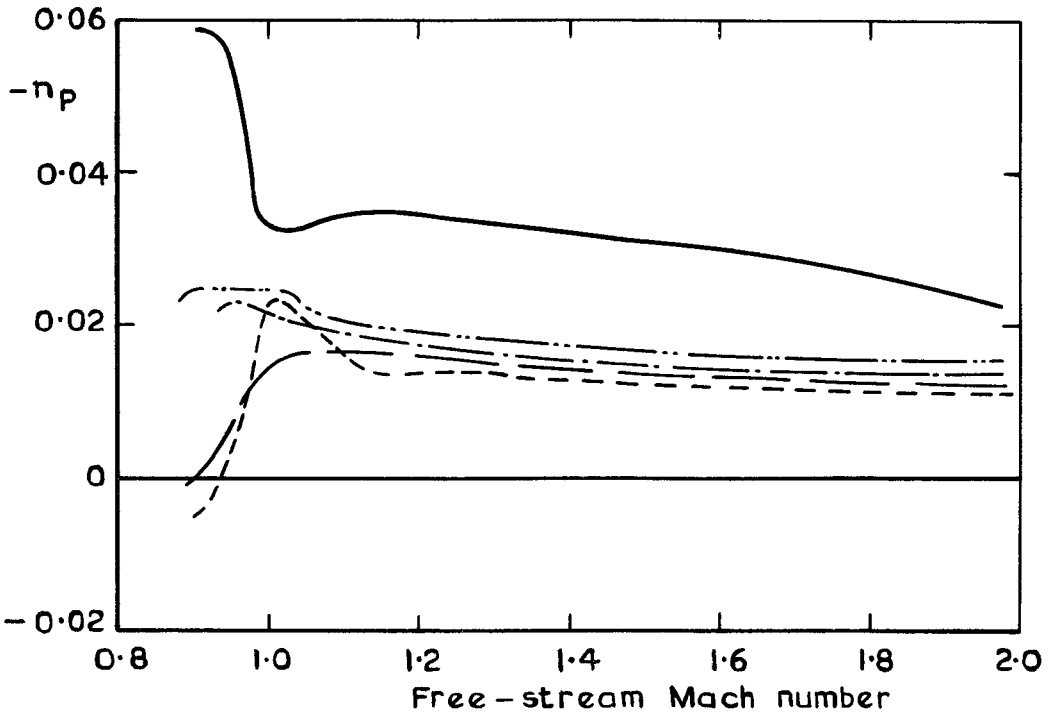

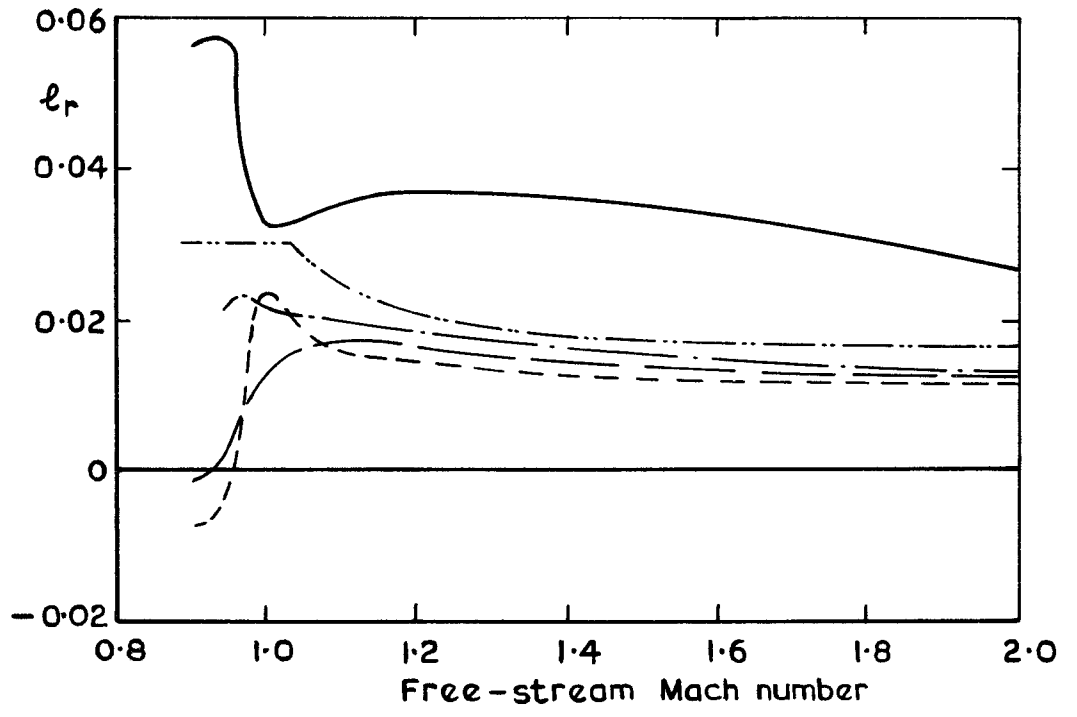

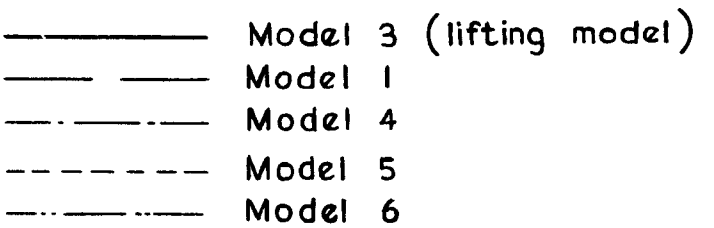

Fig. 8 Estimated derivatives n_p and ℓ_r used in the analysis method of Ref. 4

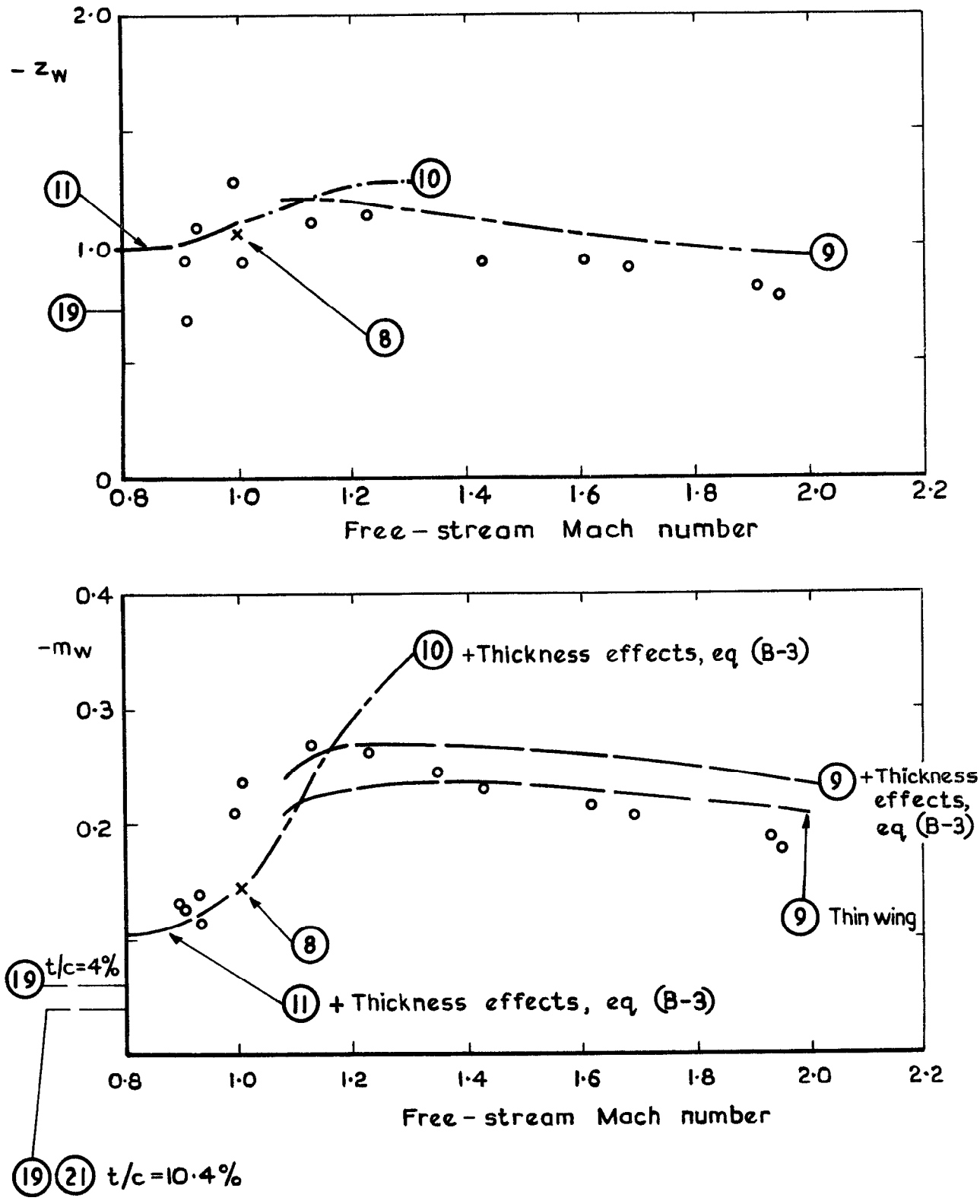

Fig. 9 z_w , m_w – basic model at zero lift

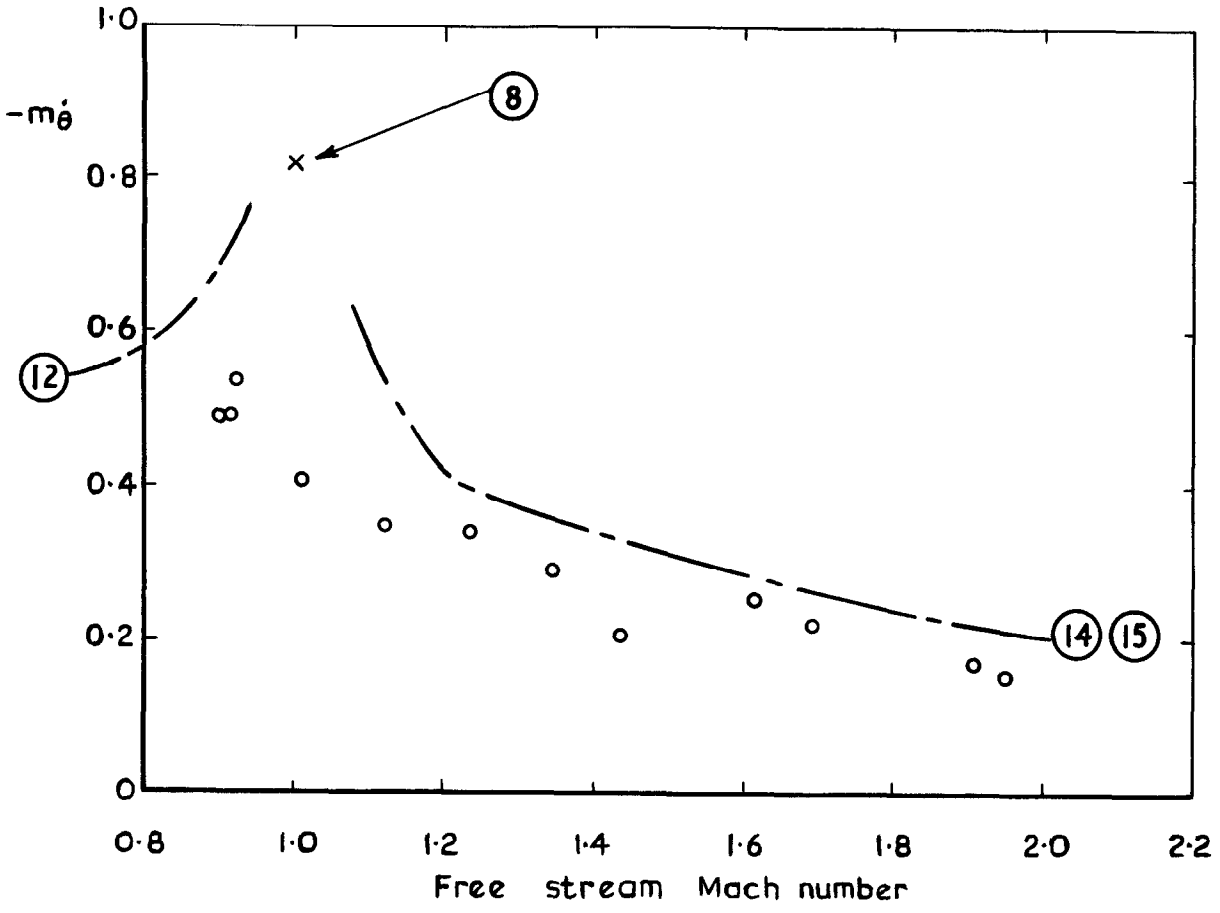

R Theory, Ref. R

Fig. 10 $m_{\dot{\theta}}$ –basic model at zero lift

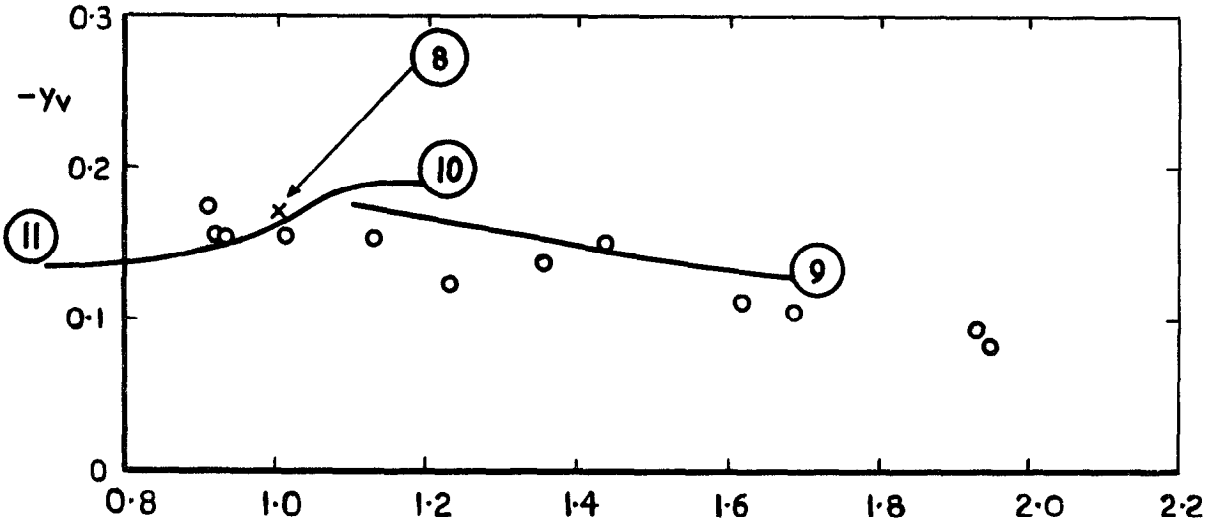

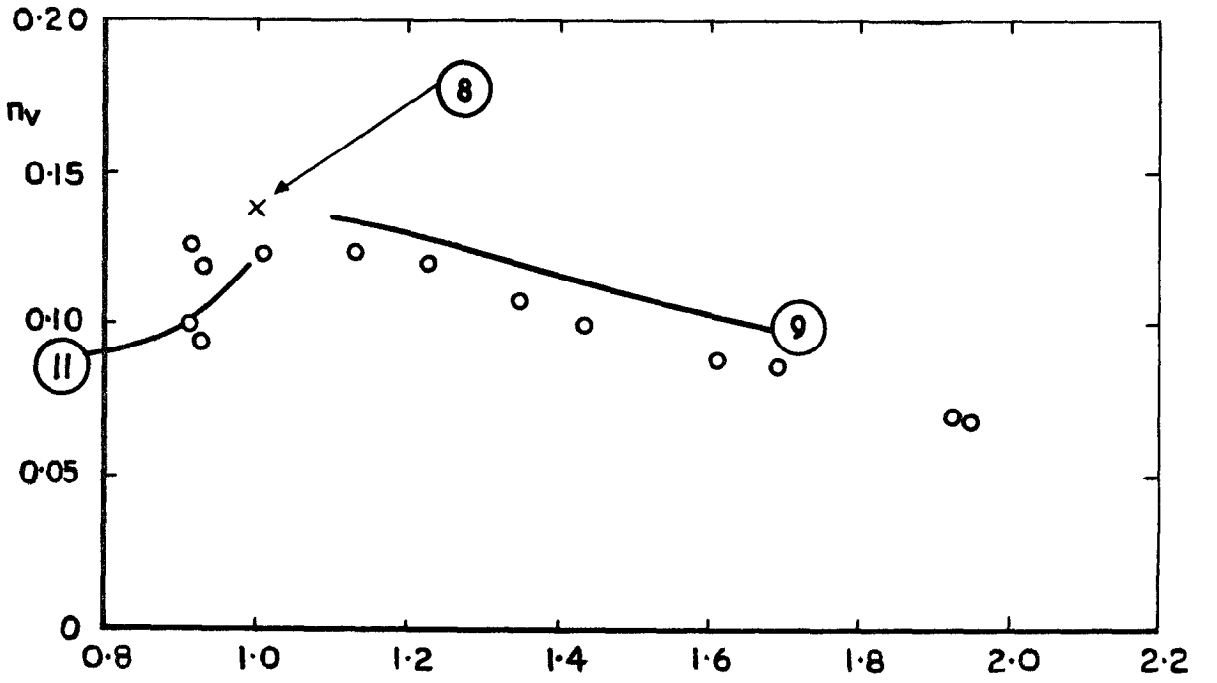

R Theory, Ref. R

Fig.11 n_v, y_v -basic model at zero lift

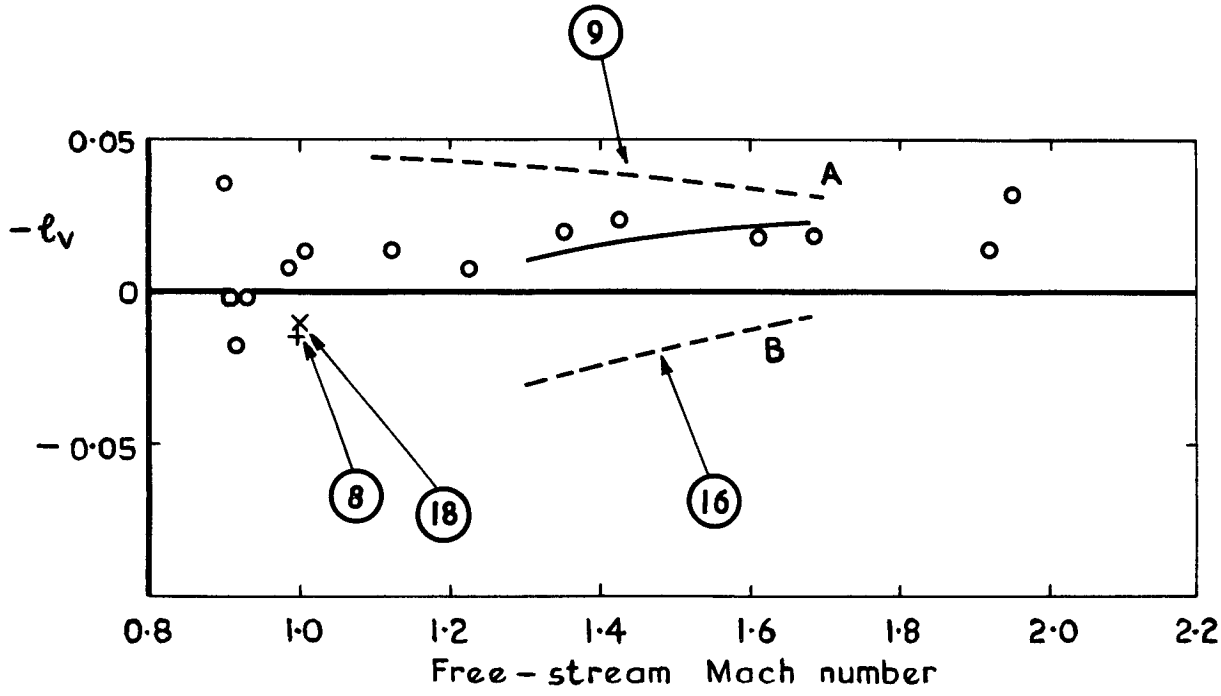

Theory { A = direct fin effect, B = wing/fin interference

Theory, resultant A+B

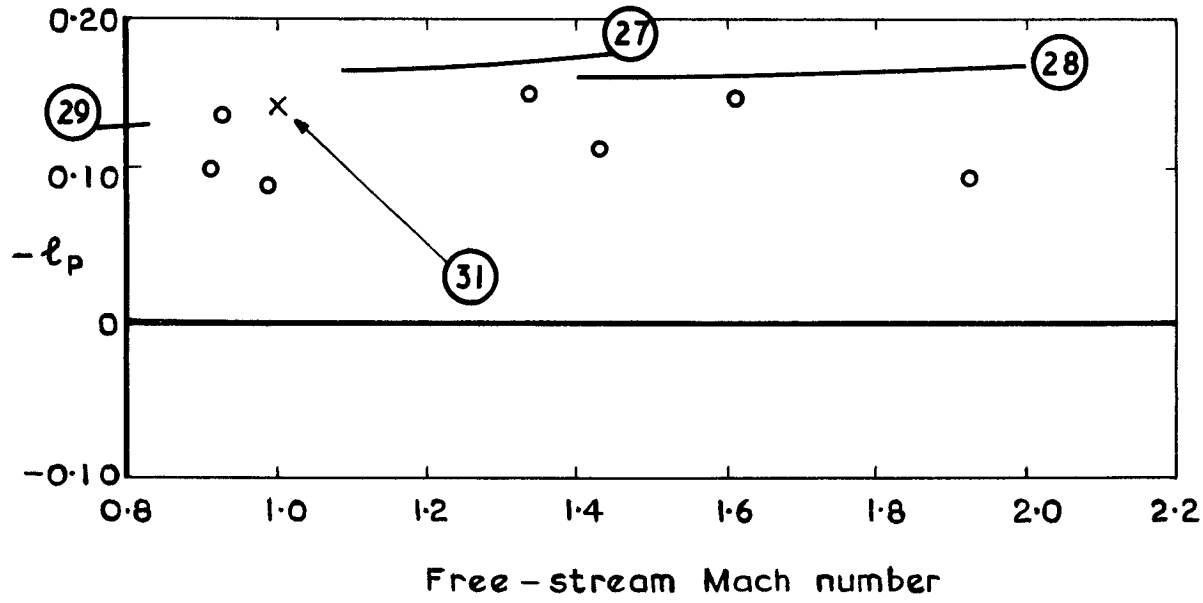

(R) Theory, Ref. R

Fig.12 ℓ_v, ℓ_p — basic model at zero lift

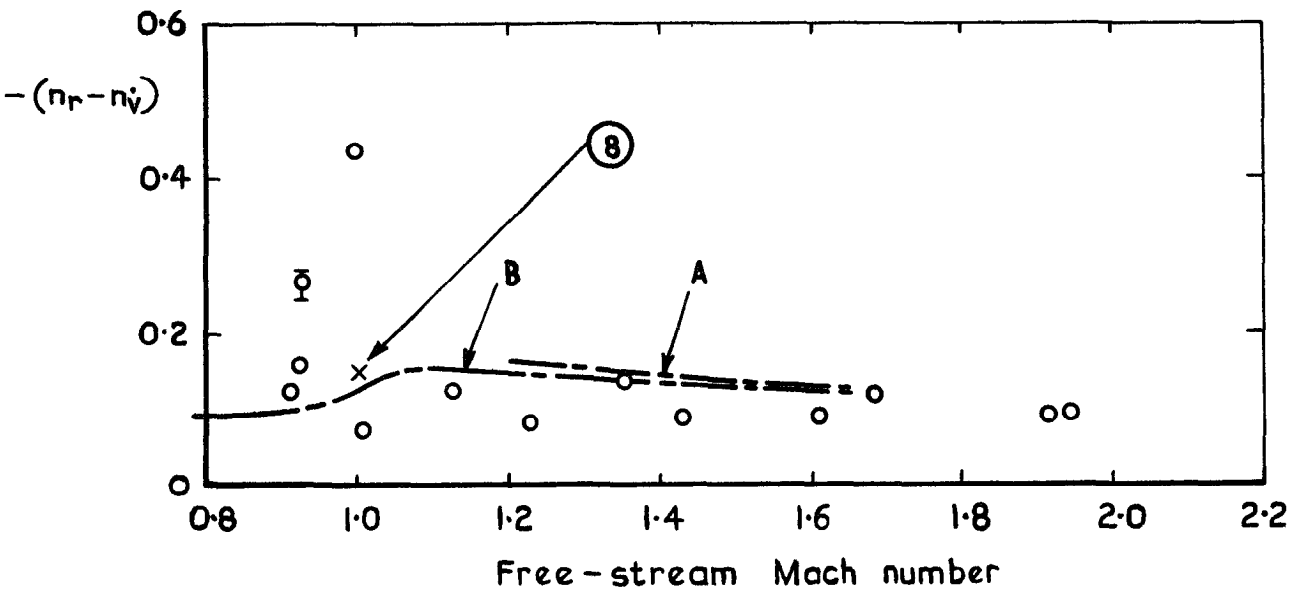

——————Theory { A = Refs. 14 and 15 eq (B-16)
B = Ref. 30 eq (B-17)

Fig.13 $(n_r - n_{\dot{v}})$ – basic model at zero lift

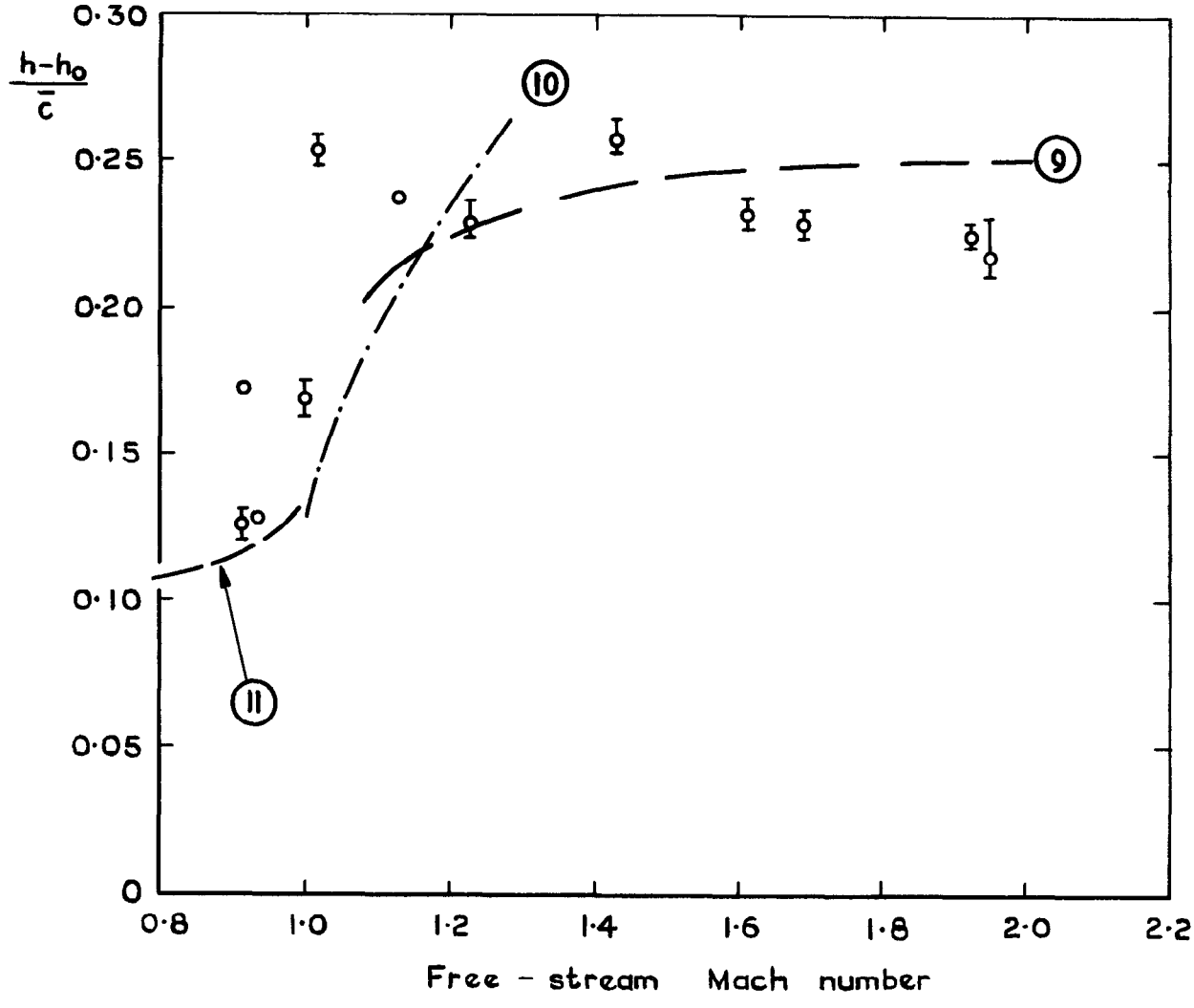

(R) Theory, Ref. R, plus thickness effects eq (B-3)

Fig. 14 Manoeuvre margin – basic model at zero lift

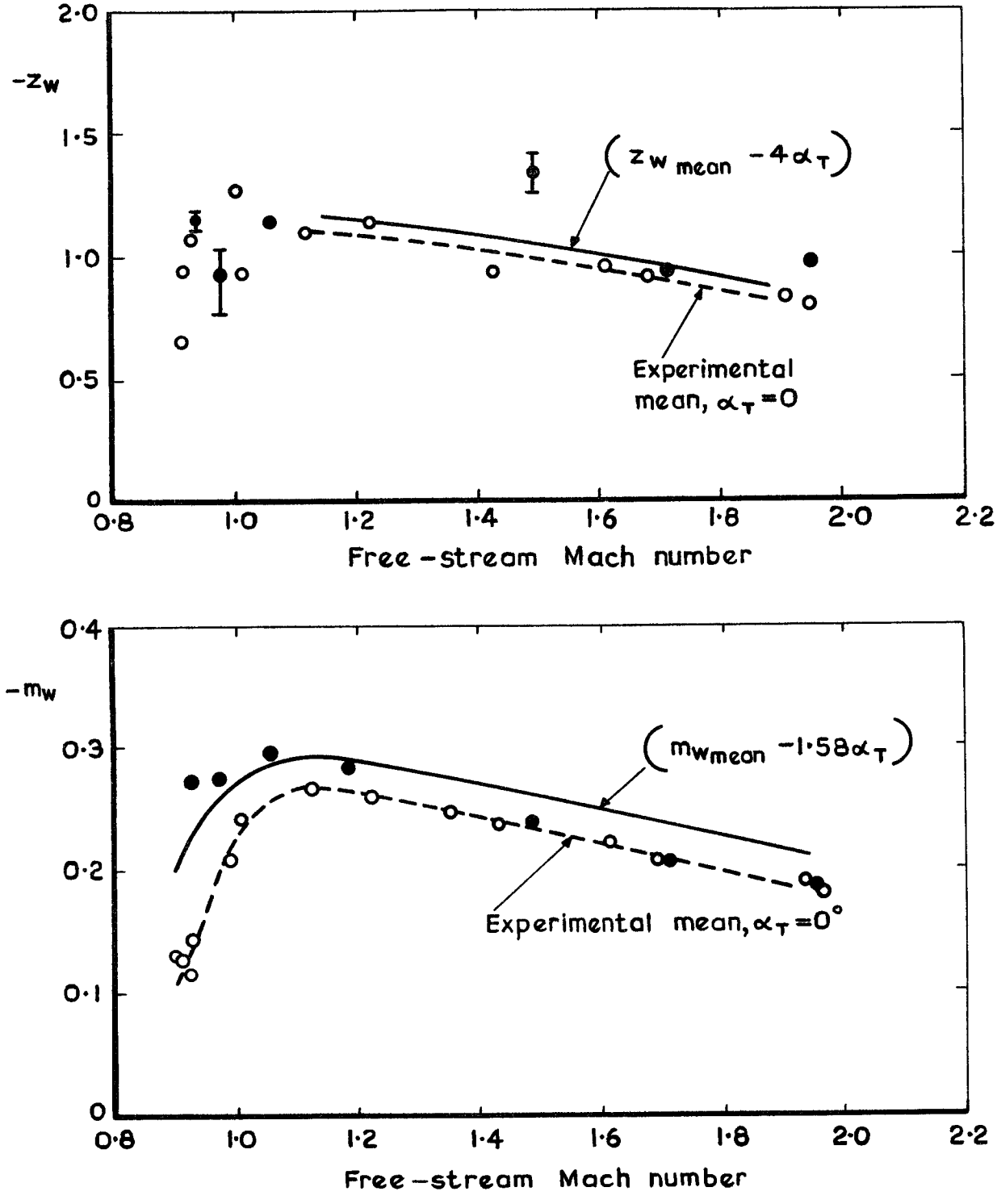

Fig.15 z_w , m_w – basic model at lift

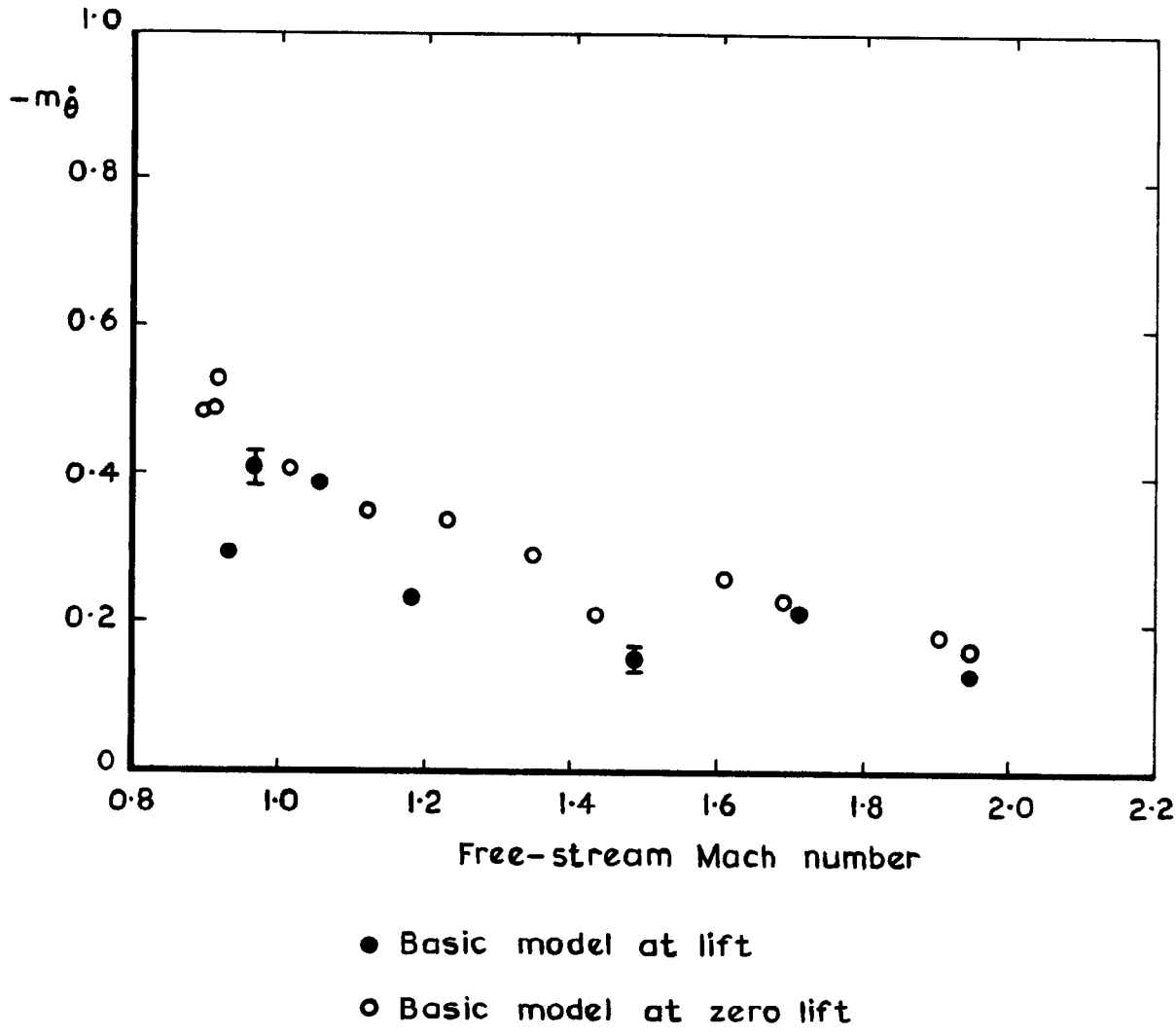

Fig.16 $m_{\dot{\theta}}$ — basic model at lift

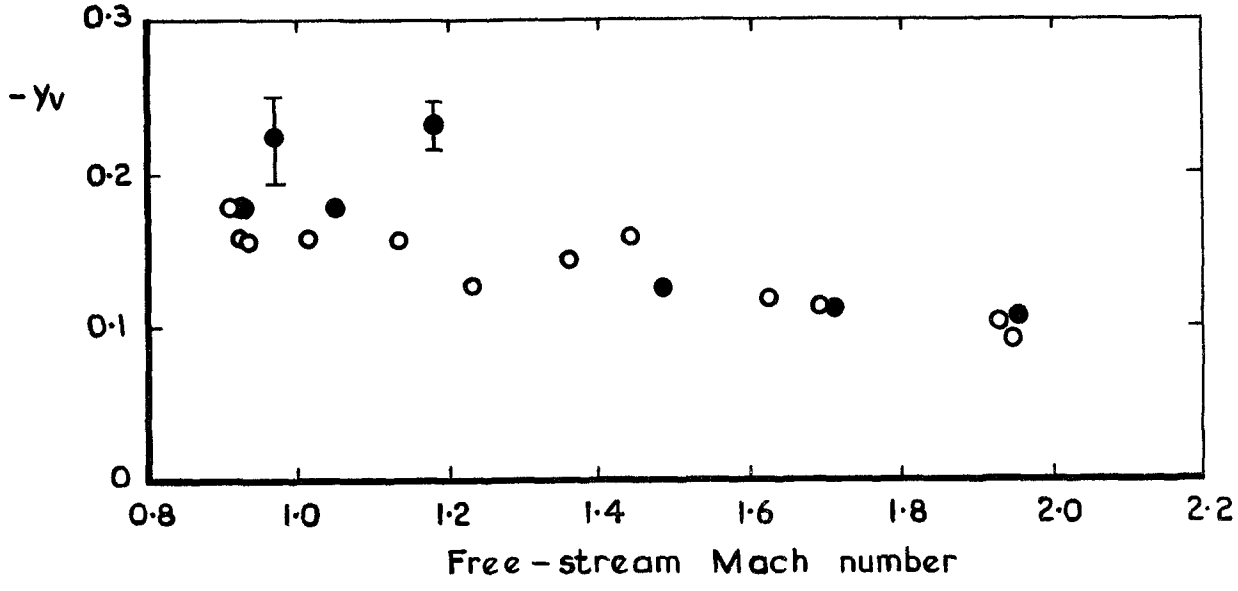

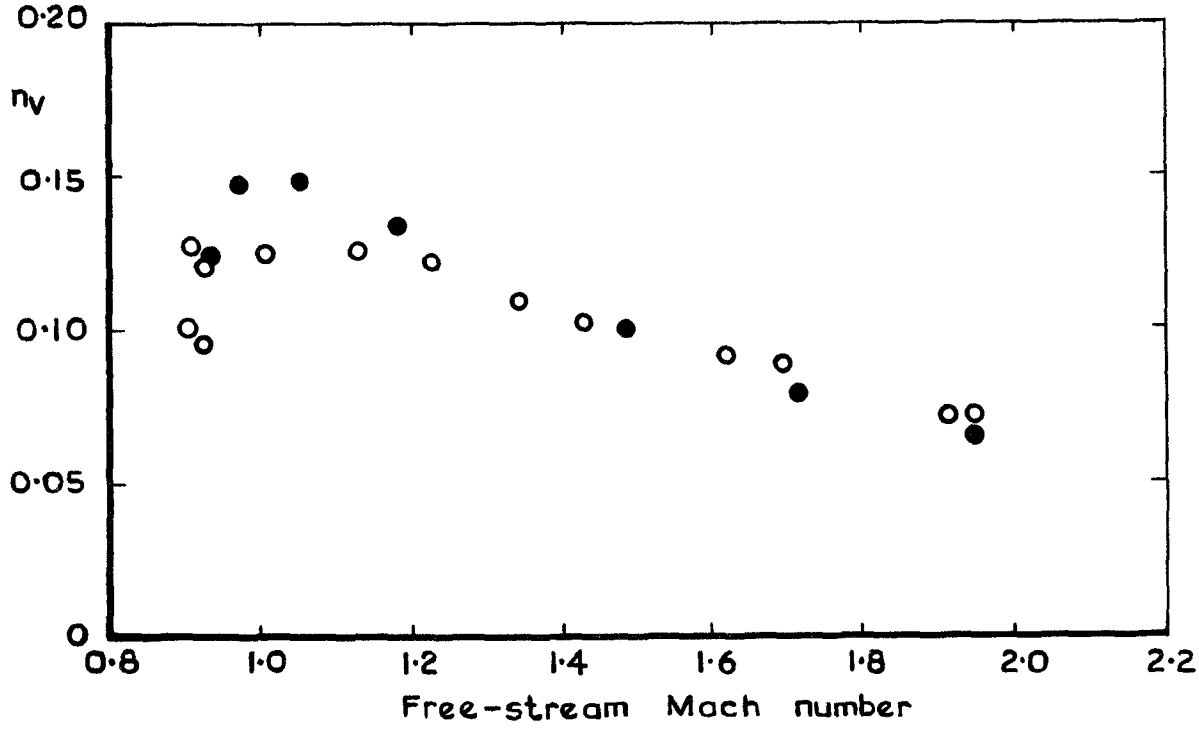

● Basic model at lift

○ Basic model at zero lift

Fig.17 n_v , y_v - basic model at lift

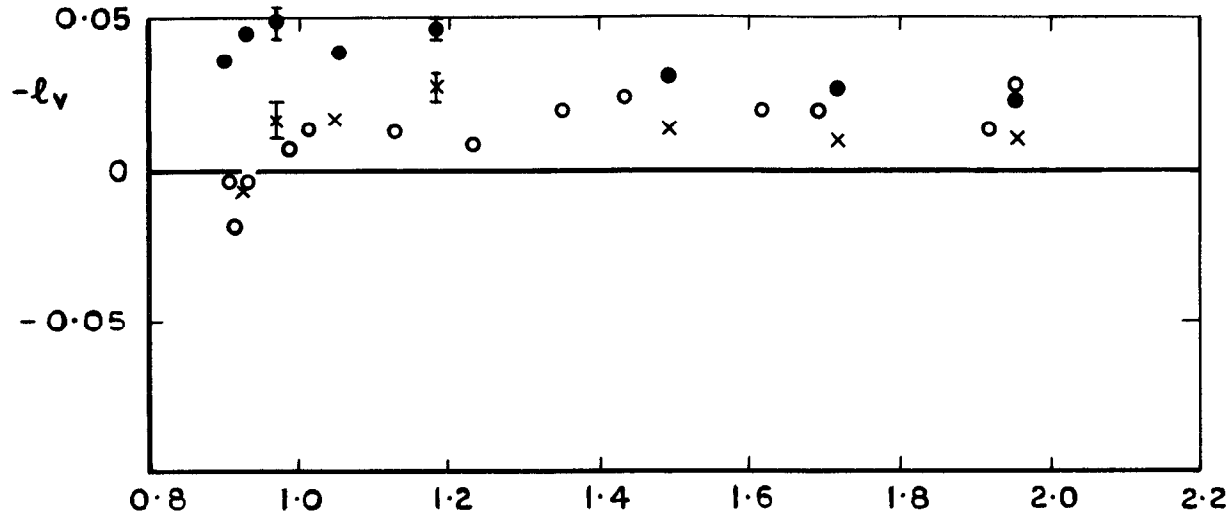

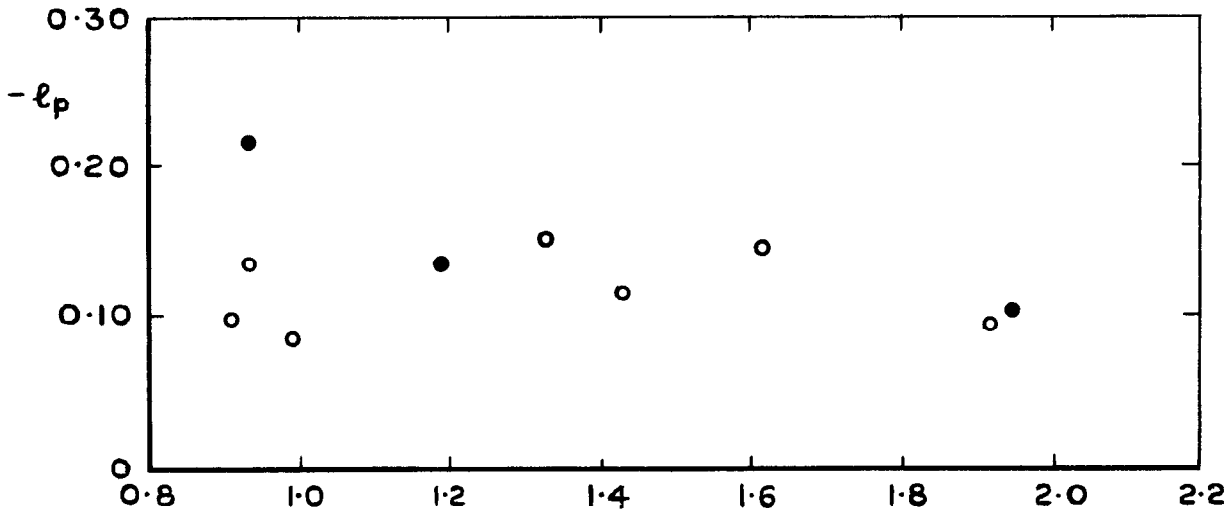

● Basic model at lift

o Basic model at zero lift

x Lifting model results reduced to zero trim angle of attack : $\ell_{v_o} = \ell_{v_{expt.}} - \ell_{v_w} \alpha_T$

Fig. 18 ℓ_v, ℓ_p — basic model at lift

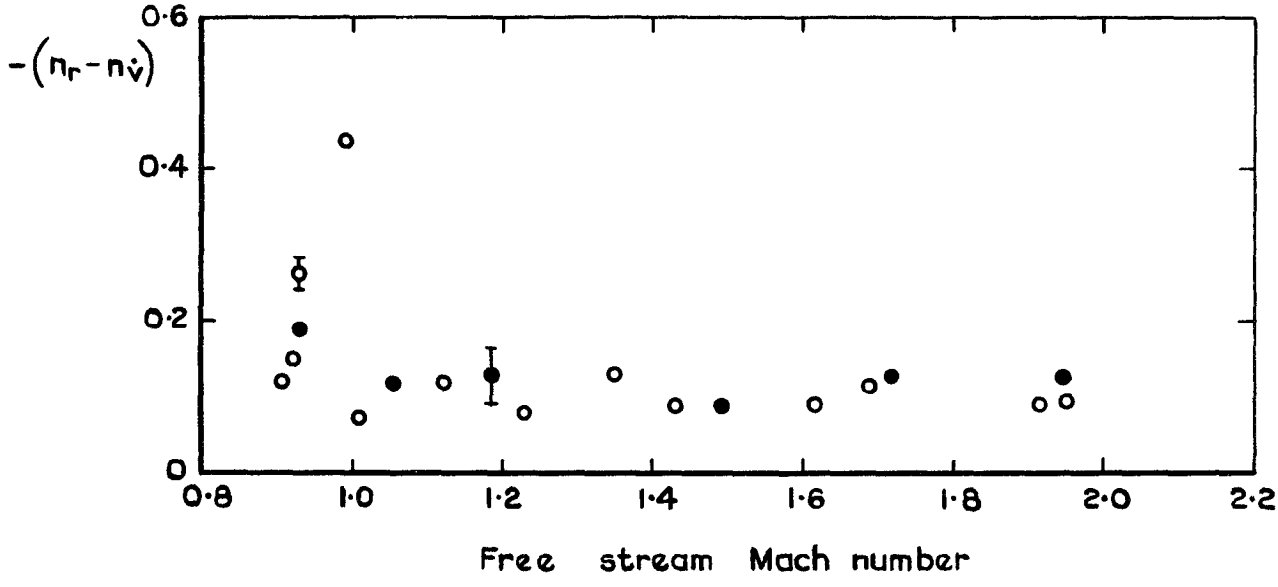

Fig. 19 $(n_r - n_{\dot{v}})$ — basic model at lift

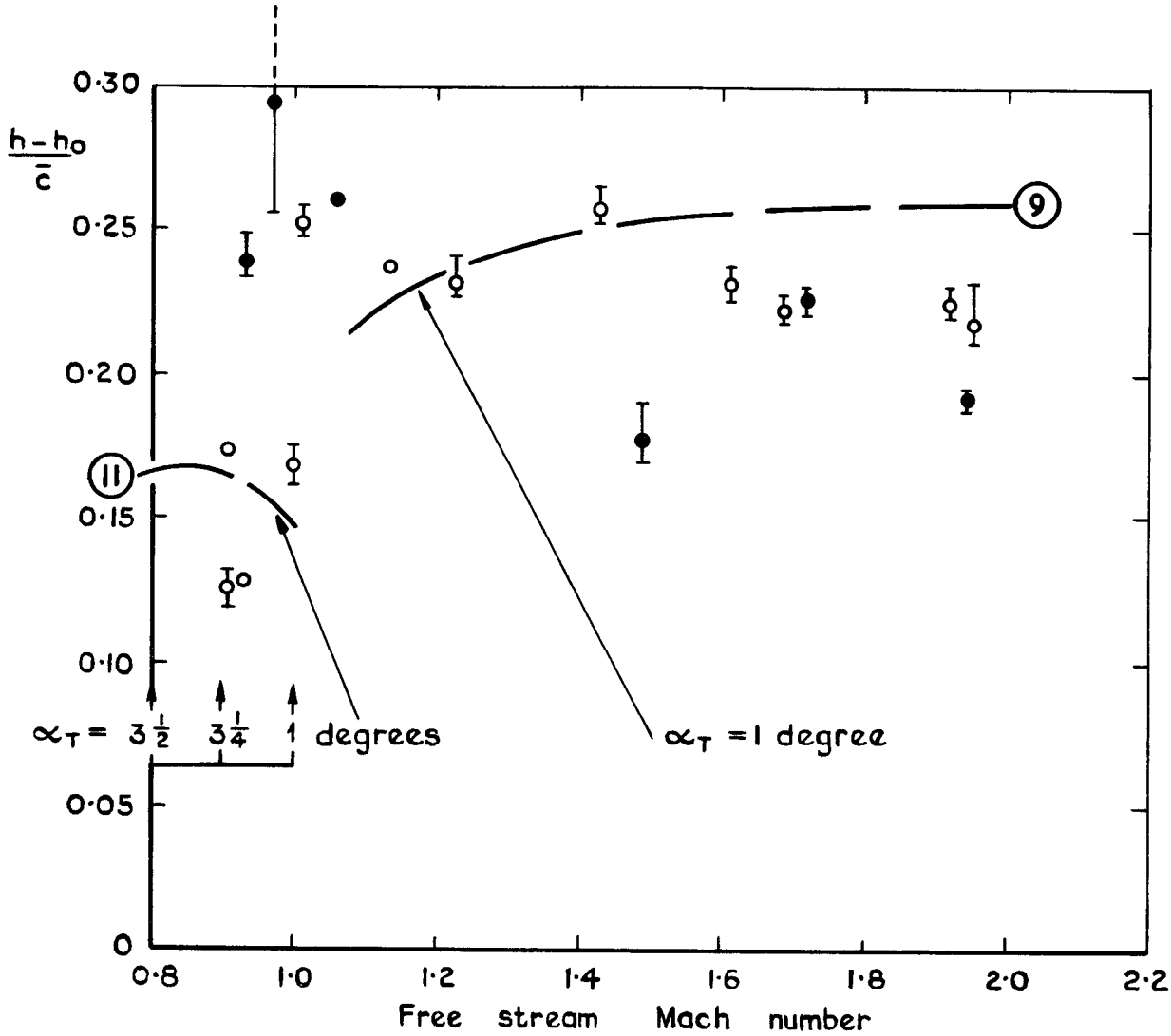

Fig.20 Manoeuvre margin – basic model at lift

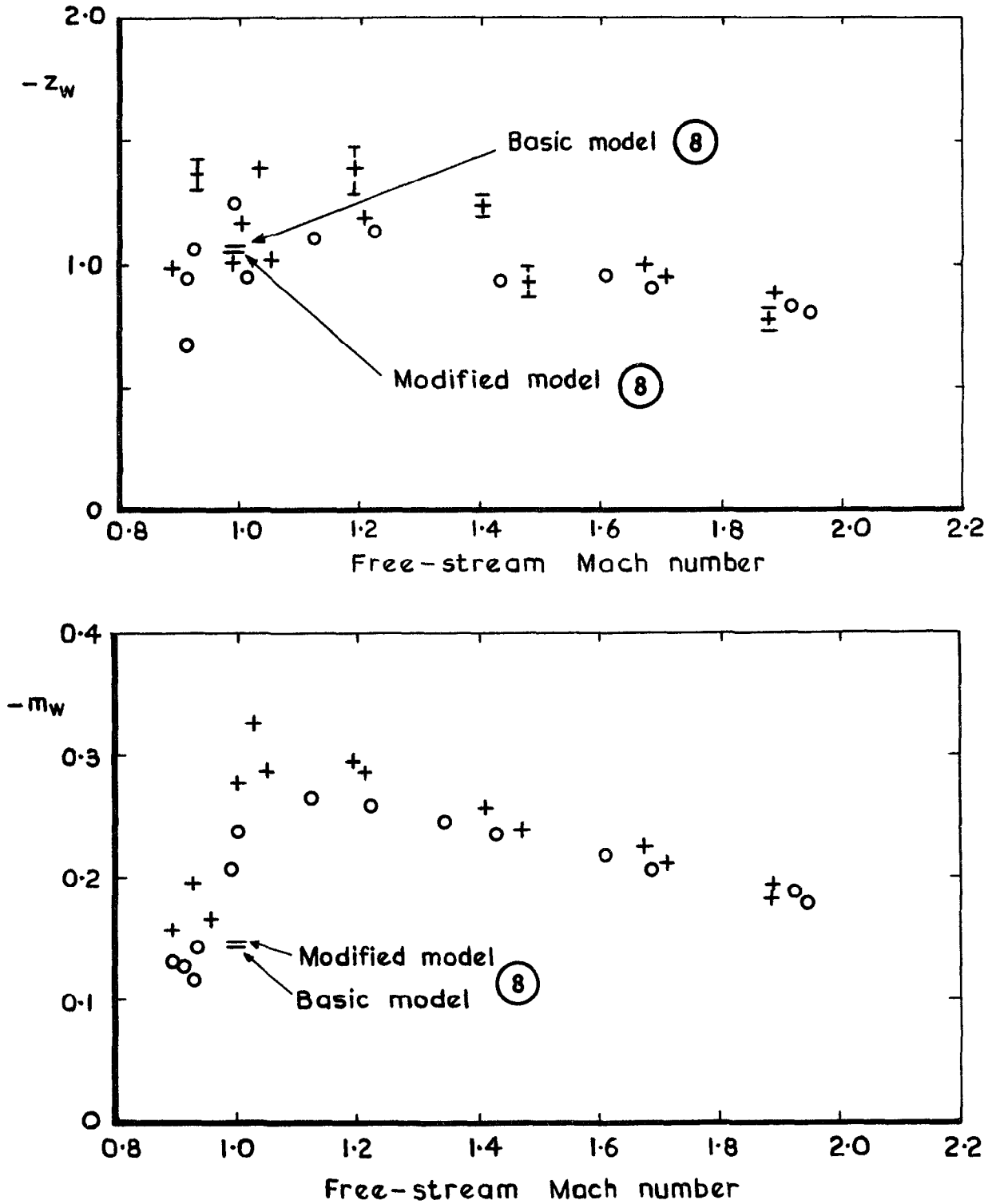

Fig. 21 z_w, m_w – modified model at zero lift

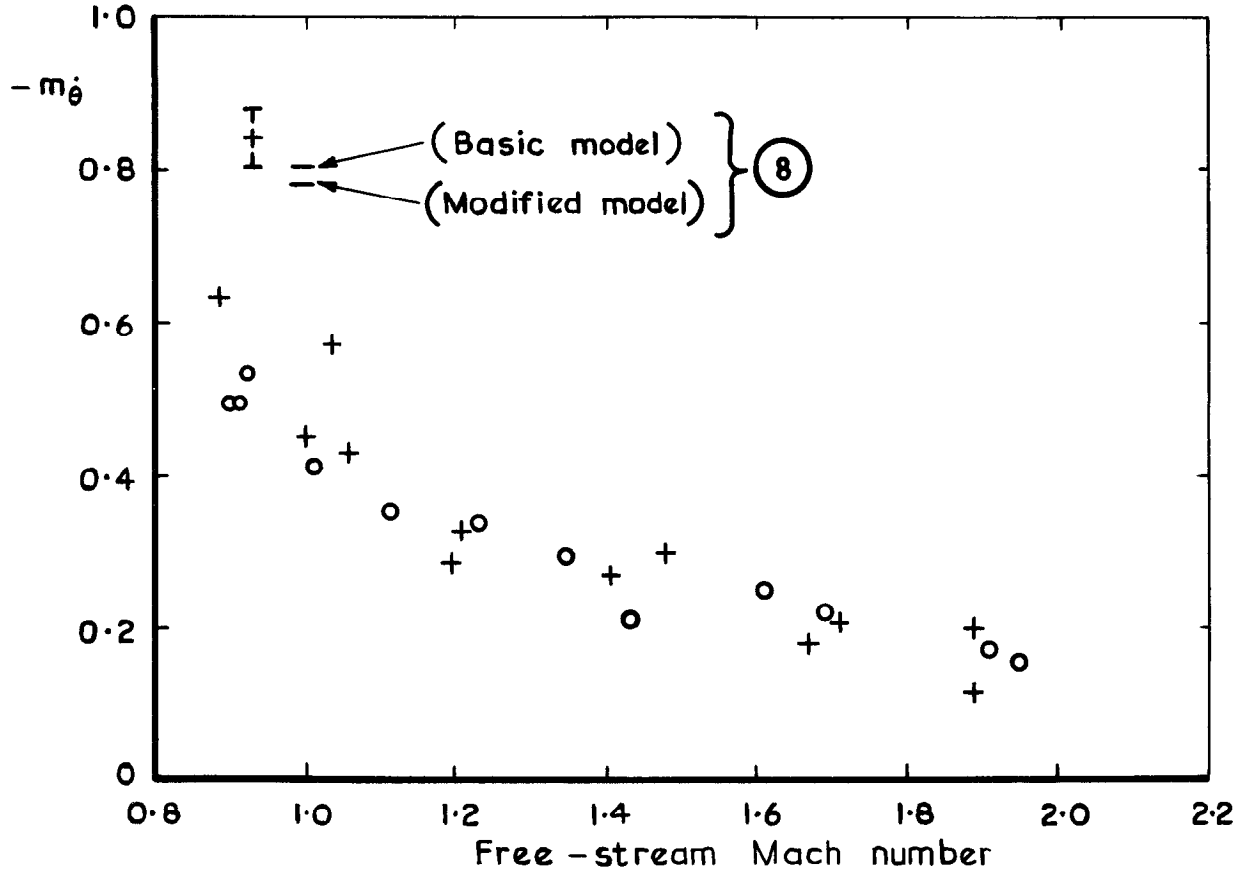

Fig. 22 $m_{\dot{\theta}}$ – modified model at zero lift

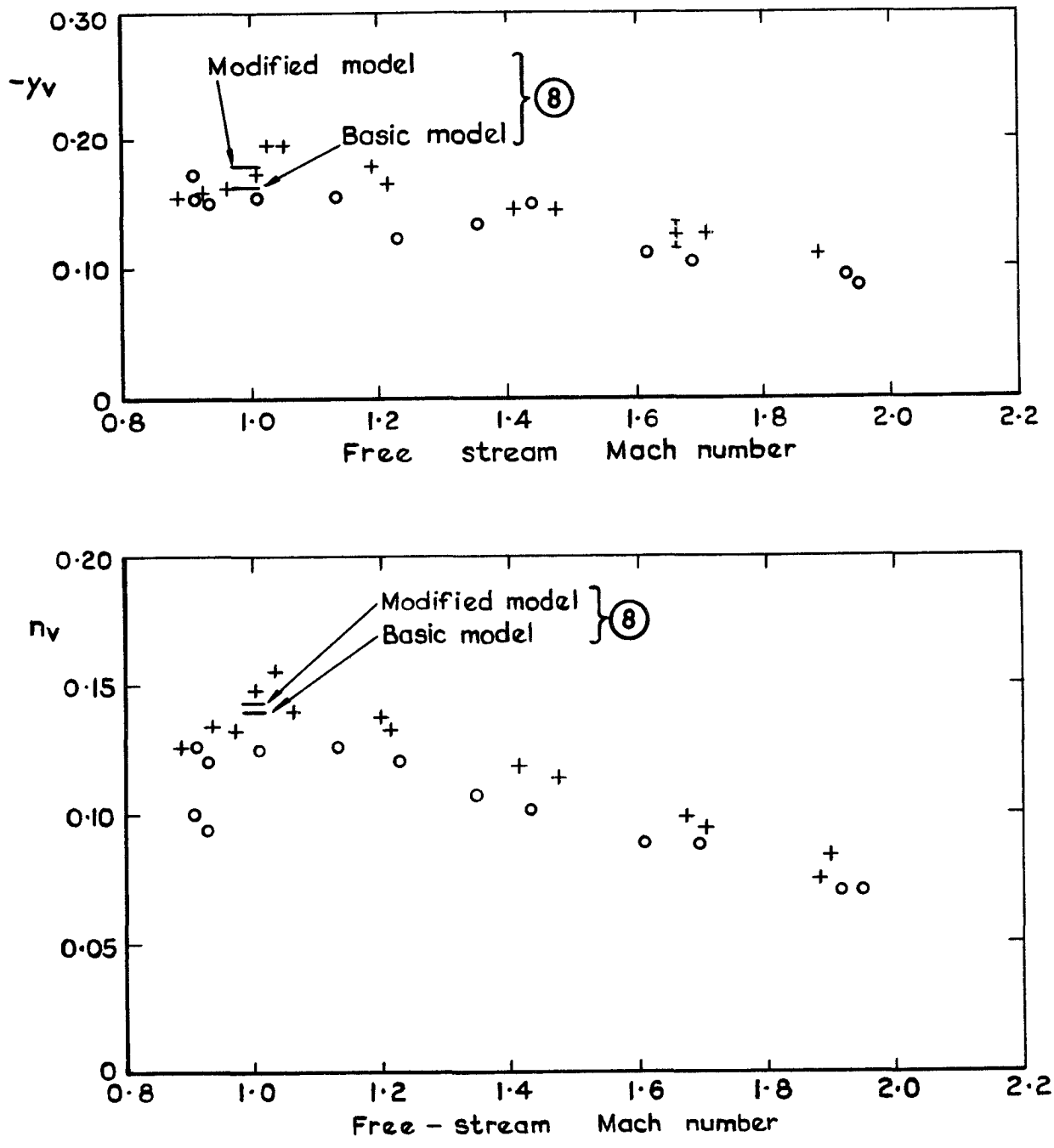

Fig. 23 n_v, y_v - modified model at zero lift

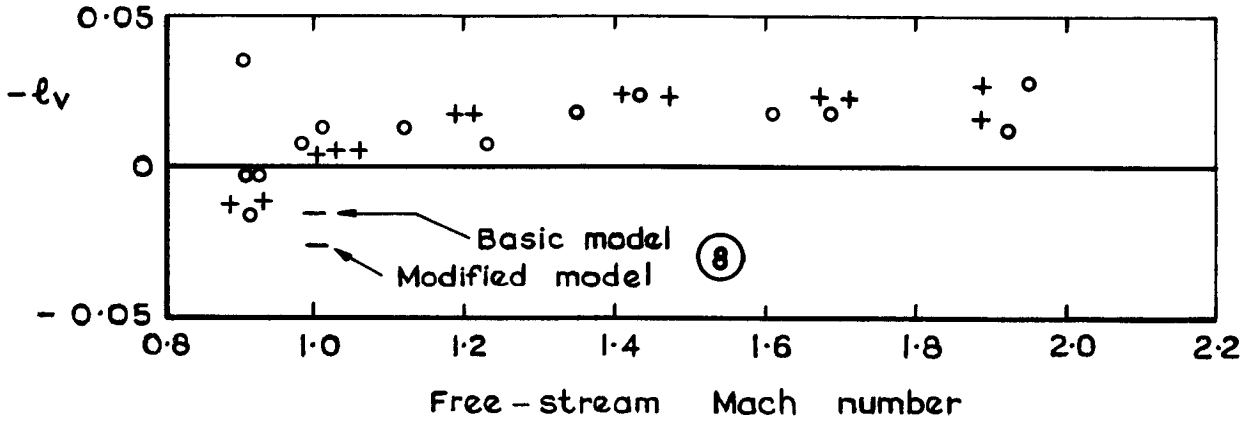

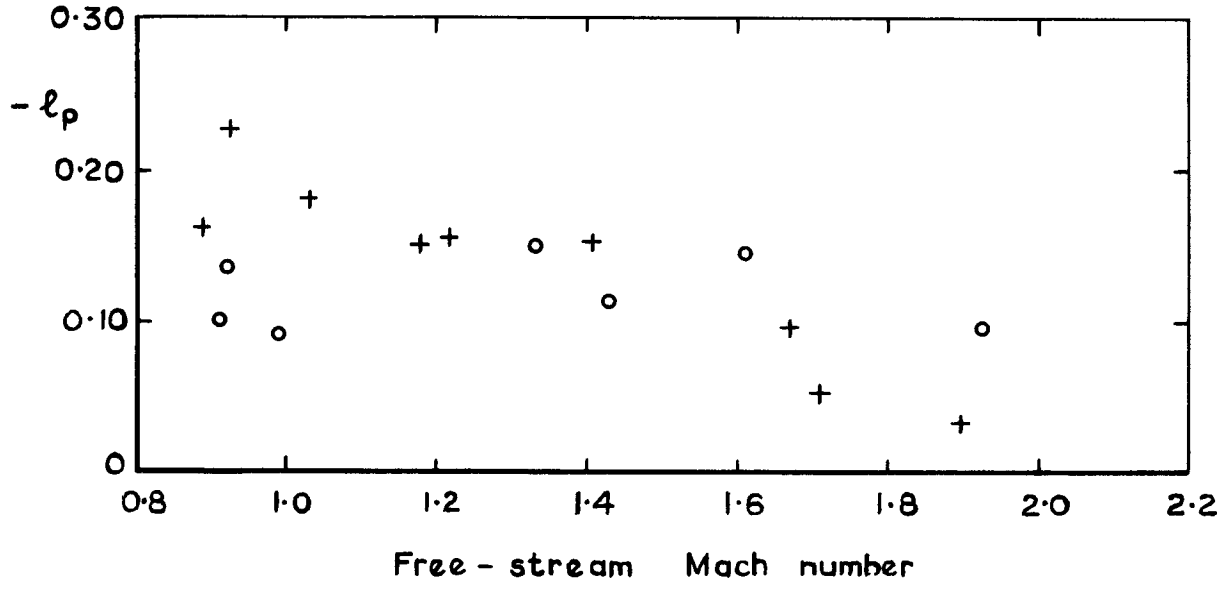

+ Modified model at zero lift

o Basic model at zero lift

Fig. 24 ℓ_v, ℓ_p — modified model at zero lift

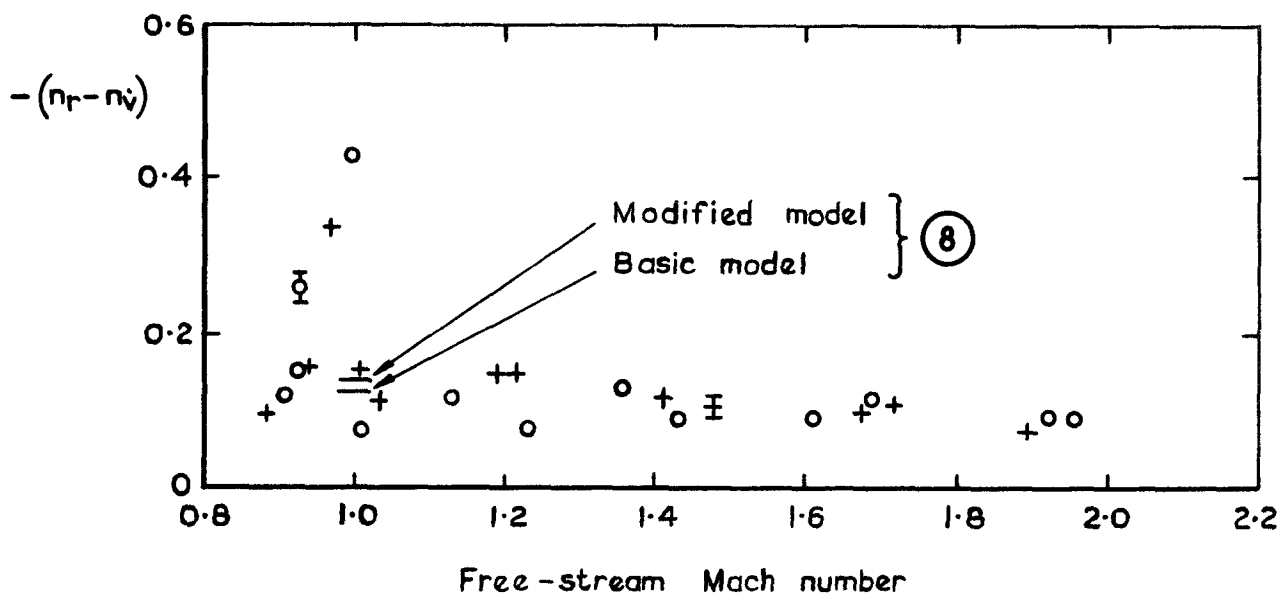

+ Modified model at zero lift

o Basic model at zero lift

Fig. 25 $(n_r - n_{\dot{v}})$—modified model at zero lift

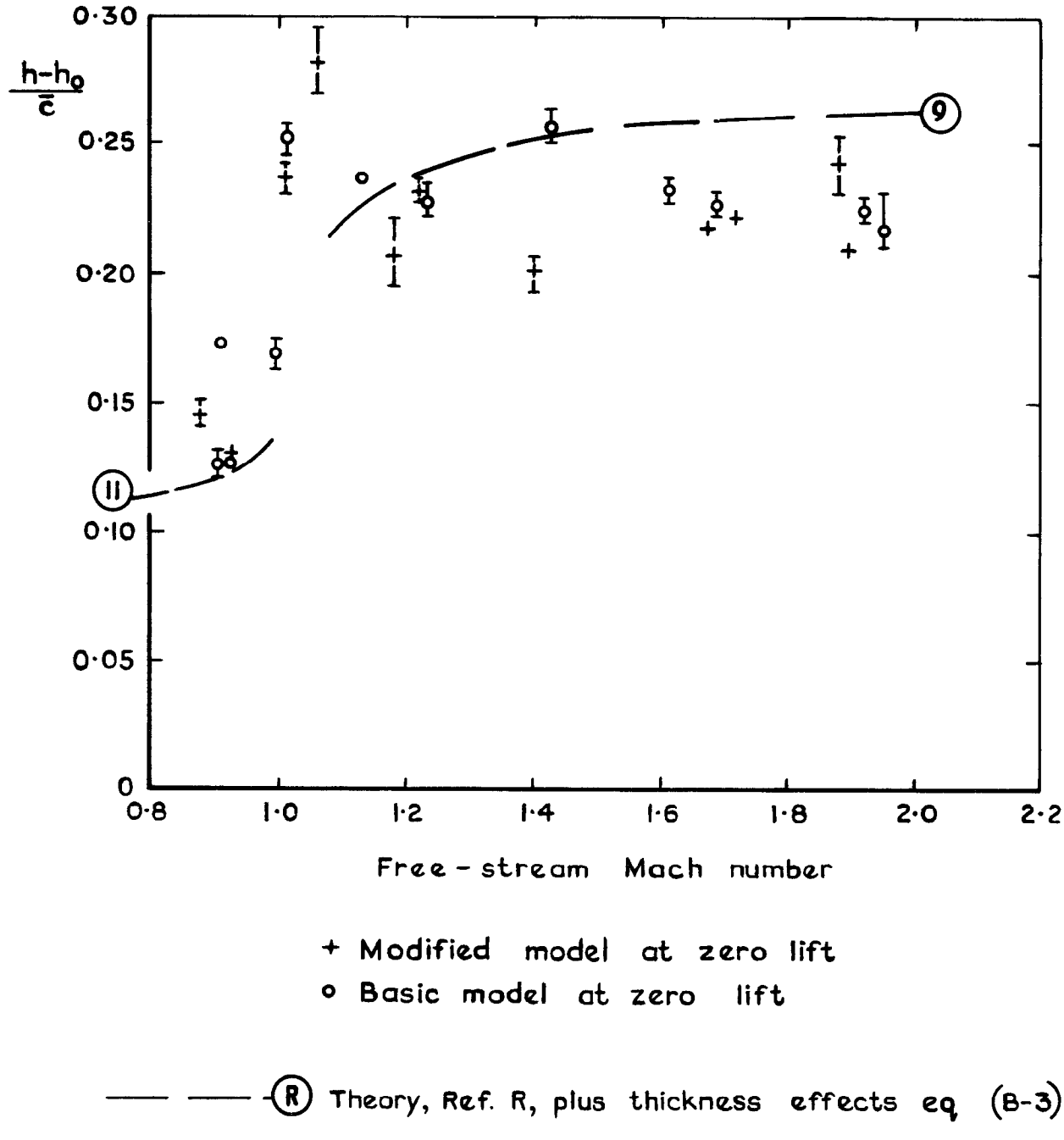

Fig. 26 Manoeuvre margin - modified model at zero lift

Printed in England for Her Majesty's Stationery Office by the Royal Aircraft Establishment, Farnborough. Dd. 505376 K4 2/75.

Published by
HER MAJESTY'S STATIONERY OFFICE

Government Bookshops
49 High Holborn, London WC1V 6HB
13a Castle Street, Edinburgh EH2 3AR
41 The Hayes, Cardiff CF1 1JW
Brazennose Street, Manchester M60 8AS
Southey House, Wine Street, Bristol BS1 2BQ
258 Broad Street, Birmingham B1 2HE
80 Chichester Street, Belfast BT1 4JY

Government Publications are also available through booksellers

C.P. No. 1315

ISBN 011 470899 1